




Article

The oxidation state and distribution of Fe in pumpellyite from the Northern Chichibu Belt in the Hijikawa district, western Shikoku, Japan

Masahide Akasaka¹ , Yumi Goishi (Imaizumi)^{1,2}, Masayuki Sakakibara³ and Yoshihiro Nakamuta⁴

¹Department of Geoscience, Interdisciplinary Graduate School of Science and Engineering, Shimane University, Nishikawatsu 1060, Matsue 690-8504, Japan;

²SHIBAURA ENGINEERING WORKS Co., Ltd., 2-5-1 Kasama, Sakae-ku, Yokohama 247-0006, Japan; ³Department of Regional Resource Management, Faculty of Collaborative Regional Innovation, Ehime University, 2-5 Bunkyo-Cho, Matsuyama 790-8577, Japan; and ⁴Kyushu University Museum, Kyushu University, Hakozaki, Higashi-ku, Fukuoka 812-8581, Japan

Abstract

Intracrystalline distribution of ferrous and ferric iron within pumpellyites ($^{\text{VII}}W_8^{\text{VI}}X_4^{\text{VI}}Y_8^{\text{IV}}Z_{12}O_{56-n}(\text{OH})_n$, $Z = 1$) from low-grade metamorphic green rocks of the Kanogawa unit in the Northern Chichibu Belt, Hijikawa district, western Shikoku, Japan, was investigated using electron microprobe analysis, X-ray Rietveld refinement, and ^{57}Fe Mössbauer spectroscopic analysis to verify the regularity of the distribution of Fe within the octahedral X and Y sites in pumpellyite and its effect on the pumpellyite structure. Two Fe-rich pumpellyite samples, labelled CLW and CHG, with average total Fe_2O_3 of 10.01 ± 1.69 and 16.07 ± 1.08 wt.%, respectively, were separated from the rock samples. The site occupancies at the X and Y sites in the CLW and CHG pumpellyites, refined using powder X-ray diffraction data, are $^X[\text{Mg}_{0.298}\text{Fe}_{0.298(5)}\text{Al}_{0.405}]^Y[\text{Fe}_{0.191}\text{Al}_{0.809}]$ and $^X[\text{Mg}_{0.244}\text{Fe}_{0.42(1)}\text{Al}_{0.34}]^Y[\text{Fe}_{0.32}\text{Al}_{0.68}]$, respectively. The $\text{Fe}^{2+}:\text{Fe}^{3+}$ ratio of the CLW pumpellyite, determined using Mössbauer spectroscopy, is 12(1):88(3). By combining the average chemical composition data, the site occupancies at the X and Y sites, and the $\text{Fe}^{2+}:\text{Fe}^{3+}$ ratio of the CLW pumpellyite, the chemical formulae of CLW and CHG pumpellyites are constructed as $(\text{Ca}_{7.96}\text{K}_{0.02}\text{Na}_{0.01})_{\Sigma 7.99}(\text{Mg}_{1.19}\text{Mn}_{0.09}^{2+}\text{Fe}_{0.39}^{2+}\text{Fe}_{0.71}^{3+}\text{Al}_{1.62})_{\Sigma 4.00}(\text{Al}_{6.47}\text{Fe}_{1.50}^{3+}\text{V}_{0.02}\text{Ti}_{0.01})_{\Sigma 8.00}\text{Si}_{12.26}\text{O}_{43.33}(\text{OH})_{12.67}$ and $(\text{Ca}_{8.01}\text{K}_{0.01})_{\Sigma 8.02}(\text{Mg}_{0.97}\text{Mn}_{0.02}^{2+}\text{Fe}_{0.63}^{2+}\text{Fe}_{1.03}^{3+}\text{Al}_{1.19})_{\Sigma 4.01}(\text{Al}_{5.44}\text{Fe}_{2.55}^{3+}\text{V}_{0.01})_{\Sigma 8.00}\text{Si}_{12.02}\text{O}_{42.69}(\text{OH})_{13.31}$, respectively, implying that the proper name of both pumpellyites is pumpellyite-(Al). The intracrystalline distribution coefficients of Fe^{3+} versus Al between the X and Y sites, $K_D = (\text{Fe}^{3+}/\text{Al})^X/(\text{Fe}^{3+}/\text{Al})^Y$, are 1.62 and 1.90 for the CLW and CHG pumpellyites, respectively, implying stronger X -site preference of Fe^{3+} than Al^{3+} . In the CHG pumpellyite, where the Fe contents at the X and Y sites are higher than in the CLW pumpellyite, the mean $\langle X-O \rangle$ and $\langle Y-O \rangle$ distances are 2.06 and 1.98 Å, respectively, which are larger than $\langle X-O \rangle = 2.040$ and $\langle Y-O \rangle = 1.944$ Å in the CLW pumpellyite. The unit-cell parameters of the CHG pumpellyite are $a = 8.8672(3)$, $b = 5.9562(2)$, $c = 19.1899(6)$ Å, $\beta = 97.473(2)^\circ$ with $V = 1004.9(2)$ Å³ and are larger than those of the CLW pumpellyite, $a = 8.8456(4)$, $b = 5.9393(2)$, $c = 19.1613(8)$ Å, $\beta = 97.461(3)^\circ$ with $V = 998.14(7)$ Å³.

Keywords: Pumpellyite-(Al); Fe in pumpellyite and juldgoldite; northern Chichibu belt in Shikoku; Mössbauer spectroscopic analysis; X-ray Rietveld analysis; crystal chemistry

(Received 8 August 2023; accepted 8 October 2023; Accepted Manuscript published online: 16 October 2023; Associate Editor: Runliang Zhu)

Introduction

Pumpellyite-group minerals are nesosorosilicate (Gottardi, 1965) with a chemical formula of $^{\text{VII}}W_8^{\text{VI}}X_4^{\text{VI}}Y_8^{\text{IV}}Z_{12}O_{56-n}(\text{OH})_n$ ($Z = 1$), where W represents cations at the seven-coordinated site, such as Ca^{2+} , K^+ and Na^+ ; X denotes divalent and trivalent cations at the octahedral site with larger site volume; Y represents trivalent cations at the octahedral sites with smaller site volume; and Z is tetrahedral Si^{4+} cations (Passaglia and Gottardi, 1973). The root name of the pumpellyite-group mineral is determined based on the most dominant trivalent cation in the Y site (Passaglia and

Gottardi, 1973): pumpellyite (with Al_Y) (Palache and Vassar, 1925), juldgoldite (with Fe_Y^{3+}) (Moore, 1971), shuiskite (with Cr_Y) (Ivanov *et al.*, 1981), okhotskite (with Mn_Y^{3+}) (Togari and Akasaka, 1987) and poppiite (with V_Y) (Brigatti *et al.*, 2006). The most dominant cation in the octahedral X site is denoted by a suffix (Passaglia and Gottardi, 1973); the root names are used in this work for simplicity.

Pumpellyite-group minerals are characteristic in low-grade metamorphic rocks subjected to zeolite- to prehnite-pumpellyite-facies metamorphism (e.g. Coombs, 1953; Passaglia and Gottardi, 1973; Liou, 1979; Schiffman and Liou, 1980; Deer *et al.*, 1986; Sakakibara, 1986, 1991; Hamada *et al.*, 2008, 2010), but also occurs in hydrothermally altered igneous rocks (e.g. Mevel, 1981; Evarts and Schiffman, 1983; Kano *et al.*, 1986; Akasaka *et al.*, 1997; Nagashima *et al.*, 2006), and ore deposits subjected to low-grade metamorphism or hydrothermal alteration

Corresponding author: Masahide Akasaka; Email: akasaka@riko.shimane-u.ac.jp

Cite this article: Akasaka M., Goishi (Imaizumi) Y., Sakakibara M. and Nakamuta Y. (2023) The oxidation state and distribution of Fe in pumpellyite from the Northern Chichibu Belt in the Hijikawa district, western Shikoku, Japan. *Mineralogical Magazine* 87, 916–934. <https://doi.org/10.1180/mgm.2023.80>

(e.g. Palache and Vassar, 1925; Togari *et al.*, 1988; Akasaka *et al.*, 1988, 1997; Minakawa, 1992). In addition, a new occurrence of okhotskite from metachert subjected to lawsonite-blueschist sub-facies metamorphism with peak metamorphic temperatures and pressures of 200–300°C and 0.6–0.8 GPa was reported by Yabuta and Hirajima (2020).

Pumpellyite-group minerals commonly contain Fe²⁺ and/or Fe³⁺ cations, and julgoldite component-rich pumpellyites are rich in Fe³⁺ (e.g. Moore, 1971; Passaglia and Gottardi, 1973; Artioli and Geiger, 1994; Akasaka *et al.*, 1997; Nagashima *et al.*, 2006). The iron content of pumpellyite depends mainly on that of the protoliths and of the metamorphic minerals coexisting with pumpellyite at each metamorphic condition, and the oxidation state of iron depends on the temperature, pressure, and *f*_{O₂} conditions of metamorphism (e.g. Coombs *et al.*, 1976; Schiffman and Liou, 1983; Togari *et al.*, 1988). Passaglia and Gottardi (1973) proposed a calculation scheme of the chemical formula and a nomenclature system of pumpellyite and julgoldite based on the crystal structure of pumpellyite clarified by Gottardi (1965) and Galli and Alberti (1969), the published chemical composition data of pumpellyites, and crystal-chemical consideration on the intracrystalline cation distributions in pumpellyite: the smallest trivalent cation, Al³⁺, is preferentially assigned to the Y site, and if Al³⁺ cations per unit cell are insufficient to fill the Y site, the second smallest Fe³⁺ is put in the Y site therein. However, detailed studies on Fe-rich pumpellyite have indicated that the distribution of trivalent cations in the octahedral sites of pumpellyite is more complicated than that estimated based on the ionic radii of trivalent cations and the volumetric sizes of the XO₆ and YO₆ octahedra. For example, in their study of pumpellyites using the methods of an X-ray Rietveld refinement and ⁵⁷Fe Mössbauer spectroscopy, Artioli and Geiger (1994) concluded selective partitioning of Fe²⁺ and Fe³⁺ cations at the X and Y sites, respectively, by assigning the two Fe³⁺-Mössbauer doublets to Fe³⁺ at the Y site, which also indicates Al³⁺ distribution in both the X and Y sites even if the amount of Al³⁺ ions is sufficient to fill the Y site; whereas, Akasaka *et al.* (1997) interpreted that two Mössbauer doublets of Fe³⁺ with larger and smaller quadrupole splits are due to Fe³⁺ in the X and Y sites, respectively, which resulted in a distribution of Fe³⁺ on both the X and Y sites and Al³⁺ on the Y site only. Artioli *et al.* (2003) also pointed out the incorrectness of the interpretation that Fe³⁺ is located exclusively at the smaller Y site. A subsequent X-ray diffraction and ⁵⁷Fe Mössbauer spectroscopic studies of Fe-rich pumpellyite by Nagashima *et al.* (2006) resulted in new pumpellyite formulae in which both Fe³⁺ and Al³⁺ are distributed at the X and the Y sites. A similar distribution of trivalent transition metal ions and Al³⁺ on the X and Y sites is also confirmed in Cr³⁺-rich pumpellyite (Nagashima and Akasaka, 2007; Nagashima *et al.*, 2010; Hamada *et al.*, 2010) and poppiite (Nagashima *et al.*, 2018), in which Cr³⁺ and V³⁺, respectively, are distributed in the two octahedral sites with Al³⁺. The distribution coefficient *K*_D of the trivalent transition metal ion, M³⁺, and Al³⁺ between the X and Y sites, is written as $K_D = [(M^{3+}/Al^{3+})^X / (M^{3+}/Al^{3+})^Y]$ (Nagashima and Akasaka, 2007; Nagashima *et al.*, 2010; Hamada *et al.*, 2010). Applying the distribution coefficient *K*_D of Fe³⁺ and Al³⁺ between the X and Y sites, $K_D = [(Fe^{3+}/Al^{3+})^X / (Fe^{3+}/Al^{3+})^Y]$, derived from the site populations after Nagashima *et al.* (2006), gives 1.12 and 1.44 (Nagashima *et al.*, 2010), indicating stronger X-site preference of Fe³⁺ than Al³⁺. The strong preference of Fe³⁺ for the larger X site seems to be reasonable because the Fe³⁺ ion has a larger ionic radius than Al³⁺ (0.645 Å for ^{VI}Fe³⁺

and 0.54 Å for ^{VI}Al³⁺ after Shannon, 1976). Moreover, the published results on the oxidation state and site distribution of Fe at the octahedral sites indicate that, although the calculation scheme of pumpellyite formula by Passaglia and Gottardi (1973) is correct in a global meaning, it does not derive a proper trivalent cation population in the octahedral X and Y sites. However, the calculation scheme of pumpellyite formula by Passaglia and Gottardi (1973) has not yet been updated to a new one.

Structural variation of pumpellyite to total Fe content in pumpellyite and to Fe distributions at the X and Y sites have also been investigated to understand the contribution of intracrystalline distribution of Fe in pumpellyite to the pumpellyite structure. As a result, the systematic changes of the structural properties, such as unit-cell parameters and the bond lengths at the X and Y sites, versus total Fe content in pumpellyite and Fe population at the X and Y sites have been proved (e.g. Allmann and Donnay, 1971; Passaglia and Gottardi, 1973; Artioli and Geiger, 1994; Akasaka *et al.*, 1997; Artioli *et al.*, 2003; Nagashima *et al.*, 2006). This made it possible to use the structural properties of pumpellyite as an index to evaluate the validity of the determined intracrystalline distribution of cations.

In addition, the intracrystalline distribution of cations and crystal structure on julgoldite have also been elucidated by several studies (e.g. Moore, 1971; Allmann and Donnay, 1973; Livingstone, 1976; Brastad, 1984; Artioli *et al.*, 2003; Nagashima *et al.*, 2018; Kasatkin *et al.*, 2021). Although the determined distributions of Fe²⁺, Fe³⁺ and Al³⁺ at the octahedral sites are somewhat variable from study to study, Artioli *et al.* (2003) and Nagashima *et al.* (2018) showed that the changes in the unit-cell parameters of julgoldite to the Fe content are consistent with the trends in pumpellyite.

Despite the contributions of the published studies on pumpellyite-group minerals cited above, precise and accurate data on the intracrystalline distribution of cations and the structural properties of pumpellyites are further required for the formulation of the crystallochemical rule on the distribution of trivalent cations in the octahedral sites of pumpellyite and its relation to the crystal structure, and for improvement of the general calculation scheme of the pumpellyite formula to one that gives realistic results.

The Kanogawa unit in the Northern Chichibu Belt, the Hijikawa district, western Shikoku, is a source of Fe-rich pumpellyite; the geology, petrology, occurrence and chemical composition of Fe-rich pumpellyite in the Hijikawa district have been reported in detail by Sakakibara *et al.* (1998), Umeki and Sakakibara (1998a) and Sakakibara *et al.* (2007). However significant new data on the crystal-chemical properties of Fe-rich pumpellyite from the Kanogawa unit (hereafter abbreviated as Kanogawa pumpellyite) has been obtained that can verify the relationship between Fe content in pumpellyite and intracrystalline cation distribution in octahedral sites, and between Fe content and features of the pumpellyite structure. Thus, in the present study, we determined the oxidation state of Fe and the cation populations at octahedral sites in the Kanogawa pumpellyite, using electron microprobe analysis (EMPA), X-ray Rietveld refinement, and ⁵⁷Fe Mössbauer spectroscopy. In this paper, we also propose a method for estimating the cation distributions at the octahedral sites and structural properties from the pumpellyite composition, based on validated systematic changes of intracrystalline cation distribution and structure versus Fe content in pumpellyite.

Study methods

Specimen

The Northern Chichibu Belt of western Shikoku, Japan, is a late Mesozoic accretionary complex adjacent to the south of the Sambagawa metamorphic belt (e.g. Kashima, 1969; Hashimoto and Kashima, 1970; Matsuoka *et al.*, 1998; Sakakibara *et al.*, 2007) (Fig. 1). In the Hijikawa district, Ozu City, Ehime Prefecture, Japan, the low-grade metamorphic rocks of the Northern Chichibu Belt are divided into Kanogawa and Hijikawa units. The former has been subjected to prehnite–pumpellyite-facies metamorphism and consists mainly of green rocks of pillow lava, dolerite and hyaloclastite, which are accompanied by chert, pebbly shale, alternating sandstone and shale, and their broken facies. The latter is composed of basic semischist, pelitic semischist, psammitic semischist, and chert that have undergone pumpellyite–actinolite-facies metamorphism (Sakakibara *et al.* 1998; Umeki and Sakakibara 1998a, 1998b; Sakakibara *et al.*, 2007). Fe-rich green pumpellyite occurs in the green rocks of the Kanogawa unit and in the basic semischist of the eastern part of the Hijikata unit (Umeki and Sakakibara, 1998a).

The rocks studied were obtained from an outcrop along the Kawabe River in the Uematsu area belonging to the Kanogawa

unit (Fig. 1). Thin sections of the rock samples were prepared for petrographic observation and chemical analysis of constituent minerals using an electron microprobe. On the basis of the occurrence and chemical composition of pumpellyite, two rock hand specimens with dark reddish-green and green colour, labelled as CLW and CHG, respectively, were selected for the preparation of pumpellyite samples used for X-ray diffraction and Mössbauer spectroscopic studies. The CLW rock sample has an intersertal texture in which clinopyroxene, hematite and hornblende fill the interstices between plagioclase phenocrysts, and contains the veinlets consisting of metamorphic minerals, such as pumpellyite + quartz, pumpellyite + chlorite + quartz + calcite, and pumpellyite + quartz + calcite. Pumpellyite occurs as needle-like crystals < 0.2 mm in length and 0.01 mm in width, showing green to pale green pleochroism, and forms a comb structure in pumpellyite–quartz veinlets (Fig. 2a) or radial aggregates. In the pumpellyite + chlorite + quartz + calcite veinlets, pumpellyite is associated closely with chlorite (Fig. 2b). The occurrences and texture of pumpellyite and associated metamorphic minerals of the CGH green rock are similar to those of the CLW green rock. Pumpellyite forms veinlets with quartz and calcite (Fig. 2c) and occurs as a replacement phase of primary minerals or as radial aggregates of fine needles.

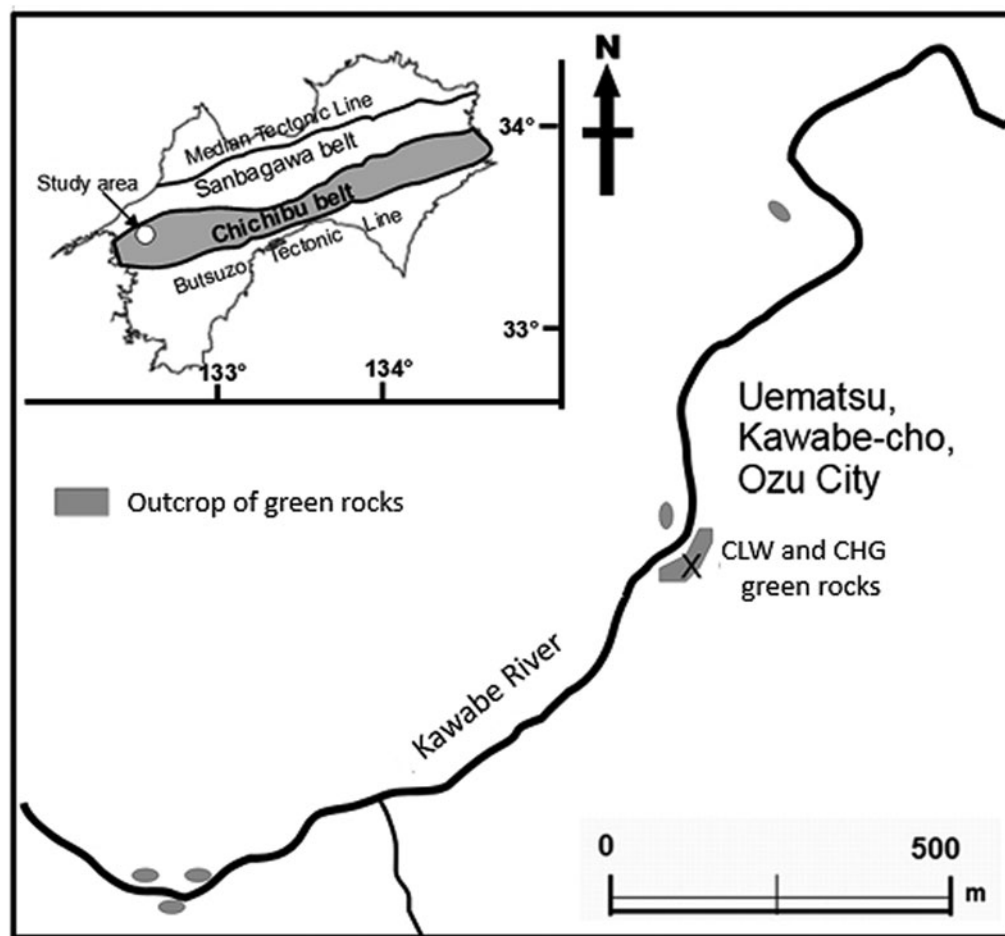


Figure 1. Sample locality map for the green rocks of Kanogawa unit, the Northern Chichibu Belt of western Shikoku, Japan, containing Fe-rich pumpellyites. The cross-mark indicates the sample point of the CLW and CHG green rocks from which the Fe-rich pumpellyites studied were separated. Inset: location of the study area and Chichibu belt in Shikoku, Japan (Umeki and Sakakibara, 1998b).

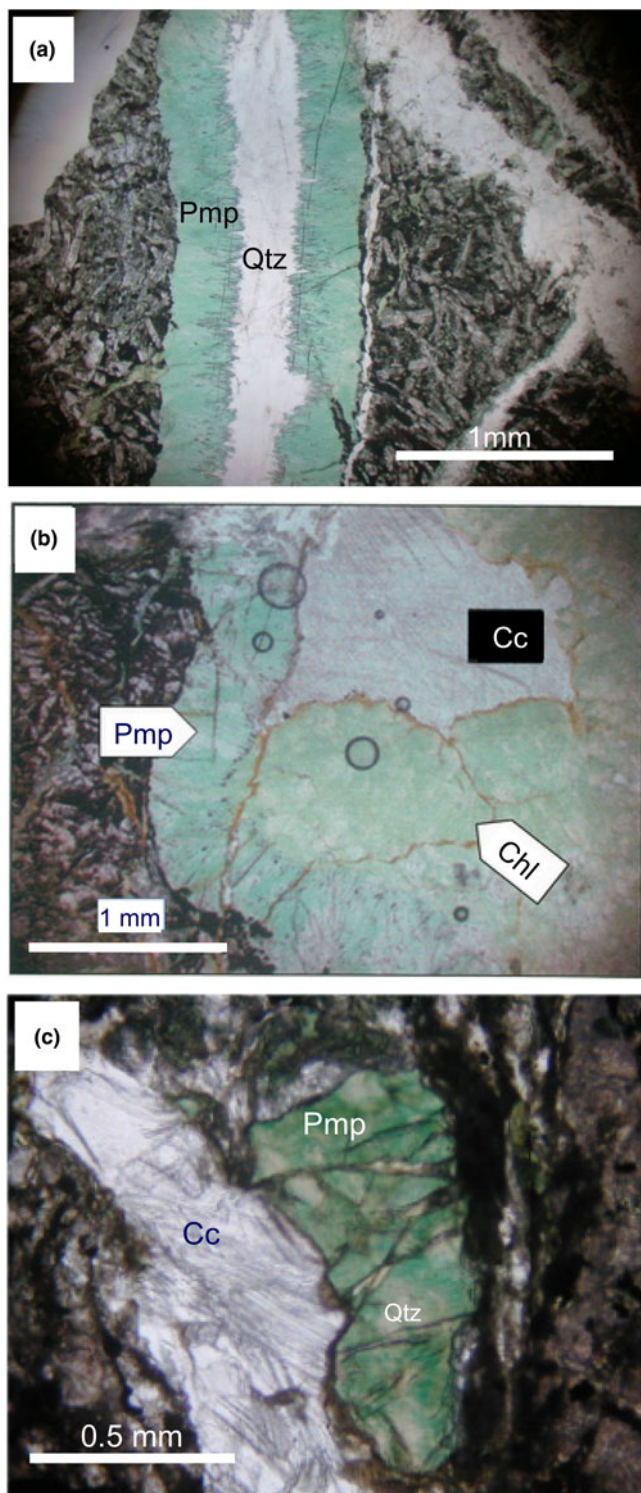


Figure 2. Microscopic photographs of pumpellyite and associated minerals in the CLW specimen (a and b) and CLG (c) (parallel-polarised light). Pmp, pumpellyite; Chl, chlorite; Cc, calcite; Qtz, quartz.

Pumpellyite samples were separated from the CLW and CHG green rock specimens by the following procedures: ~2 mm thick chips of the pumpellyite-rich part of the rock specimens were treated with dilute hydrochloric acid for the decomposition of calcite; the pumpellyites in the chips were scraped off with a marking needle and were further selected under a binocular microscope.

However, as shown in the ‘Results’ section, the pumpellyite sample separated from the CLW green rock for the X-ray diffraction analyses contained small amounts of quartz and hornblende, and that of the Mössbauer spectroscopic analysis minor chlorite. In contrast, the pumpellyite sample separated from the CHG green rock was too small in quantity for conventional powder X-ray diffraction measurement and Mössbauer spectral analysis. Thus, powder X-ray diffraction data of pumpellyite in the CHG green rock were obtained from a fragment of the pumpellyite aggregate using a Gandolfi camera (Gandolfi, 1967) and imaging plate system (Nakamuta, 1993, 1999) and a Mössbauer spectroscopic measurement was not performed. Hereafter, the pumpellyite samples separated from the CLW and CHG rock samples are designated as CLW and CHG pumpellyites, respectively.

Chemical analysis of pumpellyite

A JEOL JXA-8800M electron microprobe analyser equipped with a wavelength-dispersive X-ray spectrometer and with LiF, PET and TAP monochromator crystals was used for the chemical analysis of pumpellyite in thin sections at the operating conditions of an accelerating voltage of 15 kV, with a beam current of $2.00 \cdot 10^{-8}$ A and beam diameter of 1 μm . The standards used were: natural wollastonite for Si and Ca; synthetic TiO_2 for Ti; synthetic MgAl_2O_4 spinel for Al and Mg; synthetic Cr_2O_3 for Cr; synthetic $\text{Ca}_3\text{V}_2\text{O}_8$ for V; synthetic hematite for Fe; synthetic MnO for Mn; synthetic NiO for Ni; and natural anorthoclase for Na and K.

Four natural minerals (clinopyroxene, kaersutite, pyrope and uvarovite) with known compositions were used as working standards to monitor the precision and accuracy of the analyses. The ZAF method was used for data correction for all elements.

^{57}Fe Mössbauer spectroscopic analysis

The ^{57}Fe Mössbauer spectrum of the CLW pumpellyite was measured at room temperature, using 370 MBq ^{57}Co in Pd as a source. The data were obtained using a constant acceleration spectrometer fitted with a 1,024-channel analyser. The isomer shift (I.S.) was referenced to a standard metallic iron foil, which was also used to calibrate Doppler velocity. A Lorentzian fit was applied to the spectrum using the least-squares method, with line width and intensities of the component peaks of a doublet constrained to be equal. The QBMOSS program of Akasaka and Shinno (1992) was used for computer analysis. The quality of the fit was judged using the χ^2 and the standard deviations of the Mössbauer parameters. The doublets are assigned based on the I.S. and quadrupole splitting (Q.S.), and the $\text{Fe}^{2+}:\text{Fe}^{3+}$ ratio is derived by the area ratio of the Fe^{2+} and Fe^{3+} doublets, using the equation $[n(\text{Fe}^{2+})/n(\text{Fe}^{3+})] = C \times [A(\text{Fe}^{2+})/A(\text{Fe}^{3+})]$, where n , A and C are the number of cations, area ratio of the doublet, and constant, respectively. Empirically, the C constant is close to 1 (e.g. Bancroft, 1973), and, thus, is set to 1.0.

Powder X-ray diffraction measurement and Rietveld refinement

The CLW pumpellyite, ground to a size of ~10 μm using an agate mortar and pestle under alcohol, was mounted in a sample holder made of silicon, with a cavity measuring $10 \times 10 \times 0.25$ mm. Step-scan powder diffraction data were collected using a RIGAKU RINT automated powder X-ray diffractometer using a

Bragg-Brentano goniometer equipped with 1° divergence and anti-scatter slits, a 0.15 mm receiving slit and a curved graphite diffracted-beam monochromator. The normal-focus Cu X-ray tube was operated at 40 kV and 25 mA. Profiles were taken between 5° and 120°2 θ with a step interval of 0.02°2 θ , using step counting times that accumulated around five thousand counts for the strongest peak.

A separated fragment of the CHG pumpellyite, 0.1 × 0.1 × 0.05 mm in size, was mounted on a glass fibre of ~3 μ m in diameter for X-ray diffraction measurements using a 114 mm diameter Gandolfi camera at Kyushu University Museum (Nakamuta, 1993, 1999). A rotating anode X-ray generator with a Cr-anode 0.2 × 2 mm fine-filament and a V-filter was operated at X-ray tube voltage and current of 41 kV and 38 mA, respectively, for CrK α -radiation. The sample mounted on the glass fibre was rotated during the X-ray diffraction measurements. The X-ray powder diffraction patterns were recorded two-dimensionally on an imaging plate 35 mm wide and 350 mm long, and the intensity data on the imaging plate were read with a 50 × 50 μ m pixel size using a Fuji-film BAS-2500 IP scanner. Finally, the X-ray diffraction intensity data over a 2 θ range of 0 to 180° were obtained with a step interval of 0.0251°.

The crystal structure of the pumpellyites were refined using the RIETAN-FP program of Izumi and Momma (2007). Peaks were defined using the split Pearson VII function in the RIETAN-FP program. An asymmetric parameter is built into this profile function. Nonlinear least-squares calculation using the Marquardt method was followed by the conjugate direction method to check convergence at local minima (Izumi, 1993). Preferred orientation was corrected using the March–Dollase function (Dollase, 1986).

The powder X-ray diffraction data of the CLW pumpellyite sample indicated that the separated sample consists of not only pumpellyite but also small amounts of quartz and hornblende. Thus, in the Rietveld refinement of pumpellyite using the powder X-ray diffraction data of the CLW pumpellyite sample, quartz and hornblende were added to improve *R*-factors. Structural parameters of juldite, quartz and hornblende by Allmann and Donnay (1973), Kihara (1990) and Phillips *et al.* (1989), respectively, were used as the initial parameters of the three phases. In contrast, the CHG pumpellyite sample consisted solely of pumpellyite. In the structural refinements, Ca was fixed at the *W* site, Mg at the *X* site, and Si at the *Z* site on the basis of the published results of single-crystal and Rietveld structural refinements of pumpellyite-group minerals. Site occupancies of Al and Fe in the *X* and *Y* sites were refined using the following constraints: Al(*X*) = 1.0 – Mg(*X*) – Fe(*X*), Fe(*Y*) = [total Fe apfu – 4 × Fe(*X*)]/8, and Al(*Y*) = 1.0 – Fe(*Y*) where apfu = atoms per formula unit.

When structural parameters are refined using the powder X-ray diffraction data, it is possible to refine both the isotropic atomic displacement parameters and site occupancies simultaneously if the purity of the measured sample and the measured powder X-ray diffraction data are of high quality (e.g. Nagashima *et al.*, 2006; Nagashima and Akasaka, 2007; Akasaka *et al.*, 2019). However, if the quality of the measured powder X-ray diffraction data is not high enough for the simultaneous refinement of both structural parameters, and if the determination of site occupancy is the main objective, individual atomic displacement parameters are fixed routinely to reasonable values determined for similar compounds (Post and Bish, 1989). As the atomic structural parameters, especially atomic displacement

parameters, by Rietveld refinement are, in general, less accurately determined than by comparable single-crystal studies (Post and Bish, 1989), the single-crystal data are commonly used to fix the atomic displacement parameters for the Rietveld refinement of the site occupancy (Post and Bish, 1989). As the atomic displacement parameters of juldite determined by Allmann and Donnay (1973) (0.75 Å² at the *X* site; 0.55 Å² at the *Y* site) using a single-crystal X-ray diffraction method are almost the same as those reported by Nagashima *et al.* (2018) (0.789(8) Å² at the *X* site; 0.621(5) Å² at the *Y* site), the former study's isotropic atomic displacement parameters were employed as the initial values in the preliminary Rietveld refinements of the CLW and CHG pumpellyites. Finally, the isotropic atomic displacement parameters (*B*) of the CLW pumpellyite were refined using the constraints *B*(*W*2) = *B*(*W*1); *B*(*Y*) = *B*(*X*); and *B*(*O*2) to *B*(*O*11) = *B*(*O*1), whereas those of the CHG pumpellyite were fixed to those of juldite determined by Allmann and Donnay (1973).

The validity of the refined site occupancies was evaluated by the bond-valence-sum rule (Brown and Shannon, 1973) which examines a consistency between the refined site occupancies and the bond lengths determined from the refined atomic positions.

From the structural refinement results of the CLW and CHG pumpellyites, the mean <*X*–*O*> and <*Y*–*O*> distances and the site distortion parameters, i.e. the quadratic elongation < λ >, bond angle variance $\sigma_{\theta}(\text{oct})^2$ (Robinson *et al.*, 1971) and bond-length distortion index DI (Baur, 1974), of the *XO*₆ and *YO*₆ octahedra were calculated using the VESTA program by Momma and Izumi (2011). This software uses external programs

to calculate the values, where $\langle \lambda_{\text{oct}} \rangle = \frac{6}{\sum_{i=1}^6 (l_i/l_0)^2/6}$ [l_i is the length of the line in the strained state; l_0 is the centre-to-vertex distance for an octahedron with *O_h* symmetry whose volume is equal to that of the strained octahedron with bond lengths l_i];

$\sigma_{\theta}(\text{oct})^2 = \frac{12}{\sum_{i=1}^{12} (\theta_i - 90^\circ)^2/11}$ [where θ_i is the O–*M*–O angle];

and $\text{DI}(\text{oct}) = \frac{1}{6} \sum_{i=1}^6 |R_i/R_{\text{av}}|$ [where R_i is each bond length, R_{av} is average distance for an octahedron].

The crystallographic information files have been deposited with the Principal Editor of *Mineralogical Magazine* and are available as Supplementary material (see below).

Results

Chemical composition of pumpellyite

Average chemical compositions of the CLW and CHG pumpellyites are given in Table 1, with $n = 41$ and 25, respectively, where n is the number of analytical data points. The CLW and CHG pumpellyites contain 10.01 ± 1.69 and 16.07 ± 1.08 wt.% total Fe₂O₃ on average, respectively. The empirical formulae of the CLW and CHG pumpellyites calculated from the average compositions following the calculation scheme of Passaglia and Gottardi (1973) are:

$[\text{Ca}_{7.96}\text{K}_{0.02}\text{Na}_{0.01}]_{\Sigma 7.99}[\text{Mg}_{1.19}\text{Fe}_{2.46}^{2+,3+}\text{Mn}_{0.09}]_{\Sigma 3.74}[\text{Al}_{7.94}\text{Fe}_{0.03}^{3+}\text{V}_{0.02}\text{Ti}_{0.01}]_{\Sigma 8.00}\text{Si}_{12.26}\text{O}_{56-n}(\text{OH})_n$ and $[\text{Ca}_{8.01}\text{K}_{0.01}]_{\Sigma 8.02}[\text{Mg}_{0.97}\text{Fe}_{2.93}^{2+,3+}\text{Mn}_{0.02}]_{\Sigma 3.92}[\text{Al}_{6.77}\text{Fe}_{1.22}^{3+}\text{V}_{0.01}]_{\Sigma 8.00}\text{Si}_{12.02}\text{O}_{56-n}(\text{OH})_n$, respectively, where cations are calculated as total cations except for H to be 32 per O_{56-n}(OH)_{*n*}.

Table 1. Average chemical compositions of the CLW and CHG pumpellyites. (n = number of data).

Sample code	CLW $n=41$	S.D.	CHG $n=25$	S.D.
SiO ₂	37.16	0.70	35.18	0.41
TiO ₂	0.06	0.05	-	-
Al ₂ O ₃	20.42	0.98	16.76	0.78
V ₂ O ₃	0.08	0.06	0.03	0.03
Fe ₂ O ₃ *	10.01	1.69	16.07	1.08
MnO	0.33	0.08	0.08	0.04
MgO	2.46	0.46	1.91	0.15
CaO	22.53	0.29	21.81	0.30
Na ₂ O	0.02	0.02	0.04	0.02
K ₂ O	0.04	0.02	0.03	0.01
Total	93.11		91.88	
Σcations (except for H) = 32				
Si	12.26	0.12	12.02	0.09
Ti	0.01	0.01	-	-
Al	7.94	0.30	6.77	0.27
V	0.02	0.02	0.01	0.01
Fe	2.49	0.45	4.15	0.30
Mn	0.09	0.02	0.02	0.01
Mg	1.19	0.22	0.97	0.07
Ca	7.96	0.09	8.01	0.07
Na	0.01	0.02	-	-
K	0.02	0.01	0.01	0.00

* Total Fe as Fe₂O₃.

S.D. - standard deviation

Rietveld refinement

Details of X-ray diffraction data collection, Rietveld refinement, R -factors, goodness-of-fit ($S = R_{wp}/R_e$), and the Durbin-Watson d statistic are listed in Table 2. Errors are shown by estimated standard deviations of 1σ (esd). The refined powder X-ray diffraction patterns (Fig. 3) indicate that residual impurities of 8.6 mass %

Table 2. Data collection and details of structure refinement*.

Sample code	CLW	CHG
Radiation	CuK α (40 kV, 25 mA)	CrK α (41 kV, 40 mA)
2 θ scan range (°)	5–120	14.0–120.0
Step interval (°2 θ)	0.02	0.0251
No. of phases refined	4	1
Max. intensity (counts)	5111	9542
Space group	A2/m	A2/m
a (Å)	8.8456(4)	8.8672(3)
b (Å)	5.9393(2)	5.9562(2)
c (Å)	19.1613(8)	19.1899(6)
β (°)	97.461(3)	97.473(2)
V (Å ³)	998.14(7)	1004.9(2)
Z	4	4
D calc (g/cm ³)	3.25	3.30
R_B (%)	3.54	9.03
R_F (%)	2.23	6.22
R_p (%)	5.29	1.00
R_{wp} (%)	6.91	1.59
R_e (%)	5.13	1.51
S	1.349	1.011
D - Wd	1.114	0.714
Mass fraction:		
Pumpellyite	0.86	
Quartz	0.09	
Hornblende	0.05	

* Number within parentheses represent; the standard deviation (1σ) and refer to the last digit; R_B = R -Bragg factor; R_F = R structure factor; R_p = R -pattern; R_{wp} = R -weighted pattern; R_e = R -expected; S (= R_{wp}/R_e) = Goodness of fit (Young, 1993); D - Wd = Durbin-Watson d -statistic (Hill and Flack, 1987).

of quartz and 5.4 mass % of hornblende are present in the CLW pumpellyite sample and that the CHG pumpellyite sample consists of a single phase of pumpellyite. The refined unit-cell parameters are: $a = 8.8456(4)$, $b = 5.9393(2)$, $c = 19.1613(8)$ Å, and $\beta = 97.461(3)^\circ$, resulting in a cell volume of $V = 998.14(7)$ Å³, for the CLW pumpellyite; and $a = 8.8672(3)$, $b = 5.9562(2)$, $c = 19.1899(6)$ Å, and $\beta = 97.473(2)^\circ$, with $V = 1004.9(2)$ Å³, for the CHG pumpellyite, where the space group is $A2/m$.

Refined atomic positions and site occupancies are shown in Table 3. The selected bond lengths are given in Table 4. The resulting site occupancies in the X and Y sites of the CLW pumpellyite are Mg_{0.298}Fe_{0.298(5)}Al_{0.405} and Fe_{0.191}Al_{0.809}, respectively, and those of the CHG are Mg_{0.2435}Fe_{0.42(1)}Al_{0.34} and Fe_{0.32}Al_{0.68}, respectively. The Fe contents calculated from the refined site occupancies are 2.72 apfu for the CLW pumpellyite, and 4.24 apfu for the CHG pumpellyite. As the Fe contents derived from the X-ray diffraction data include minor transition elements such as Mn, V and Ti that have similar atomic scattering factors to Fe, the Fe contents of CLW and CHG pumpellyites obtained from the X-ray diffraction data, of 2.72 and 4.24 apfu, respectively, are compared with the EMPA data for CLW and CHG pumpellyite, of 2.61 apfu (= 2.49Fe + 0.09Mn + 0.02V + 0.01Ti) and 4.18 apfu (= 4.15Fe + 0.02Mn + 0.01V), respectively. Thus, the Fe contents, including minor transitional metals other than Fe, obtained from the X-ray diffraction data are reasonably consistent with the EMPA data. The results for evaluation of validity of the refined site occupancies using the bond-valence-sum rule are shown and discussed in the 'Discussion' section below.

The quadratic elongation $\langle \lambda \rangle$, bond angle variance σ_θ^2 , and bond-length distortion index DI of the XO₆ and YO₆ octahedra of the CLW and CHG pumpellyites are given in Table 5 with four significant digits based on the accuracy of the bond lengths (Table 4).

⁵⁷Fe Mössbauer spectroscopic analysis

The ⁵⁷Fe Mössbauer spectrum of the CLW pumpellyite sample is shown in Fig. 4 and the hyperfine parameters are listed in Table 6. The spectrum is composed of four doublets. On the basis of the reported ⁵⁷Fe Mössbauer hyperfine parameters on Fe of pumpellyite, i.e. I.S. = 0.29–0.38 mm/s and Q.S. = 1.06–1.12 mm/s for Fe³⁺ in the X site, I.S. = 0.35–0.37 mm/s and Q.S. = 1.9–2.1 mm/s for Fe³⁺ in the Y site (Akasaka *et al.*, 1997; Artioli *et al.*, 2003; Nagashima *et al.*, 2006), and I.S. = 1.09–1.14 mm/s and Q.S. = 3.20–3.39 mm/s for Fe²⁺ in the X site (Artioli and Geiger, 1994; Akasaka *et al.*, 1997; Artioli *et al.*, 2003; Nagashima *et al.*, 2006), the doublet AA' (I.S. = 0.31(1) mm/s and Q.S. = 1.21(2) mm/s) is assigned to Fe³⁺ at the octahedral sites. However, its broad peak width, $\Gamma = 0.56(2)$ mm/sec, indicates that the doublet AA' consists of overlapped doublets by Fe³⁺ at the X and Y sites. In most of the published Mössbauer spectroscopic studies on pumpellyite and juldite, the doublets due to Fe³⁺ at the X and Y sites have been resolved individually (e.g. Akasaka *et al.*, 1997; Artioli *et al.*, 2003; Nagashima *et al.*, 2006). However, the fitting of each doublet due to Fe³⁺ at the X and Y sites was not successful because of the strong overlap of the doublet CC' by Fe³⁺ of chlorite that remained in the separated sample. The doublet BB' with I.S. = 1.06(2) mm/s and Q.S. = 3.46(4) mm/s is assigned to Fe²⁺ at the X site. On the basis of the Mössbauer hyperfine parameter data of chlorite from De Grave *et al.* (1987), i.e. I.S. = 0.23(5) and Q.S. = 0.70(3) mm/s for Fe³⁺; and I.S. = 1.14(3)–1.16(3) and Q.S. = 2.38(5)–2.67(5)

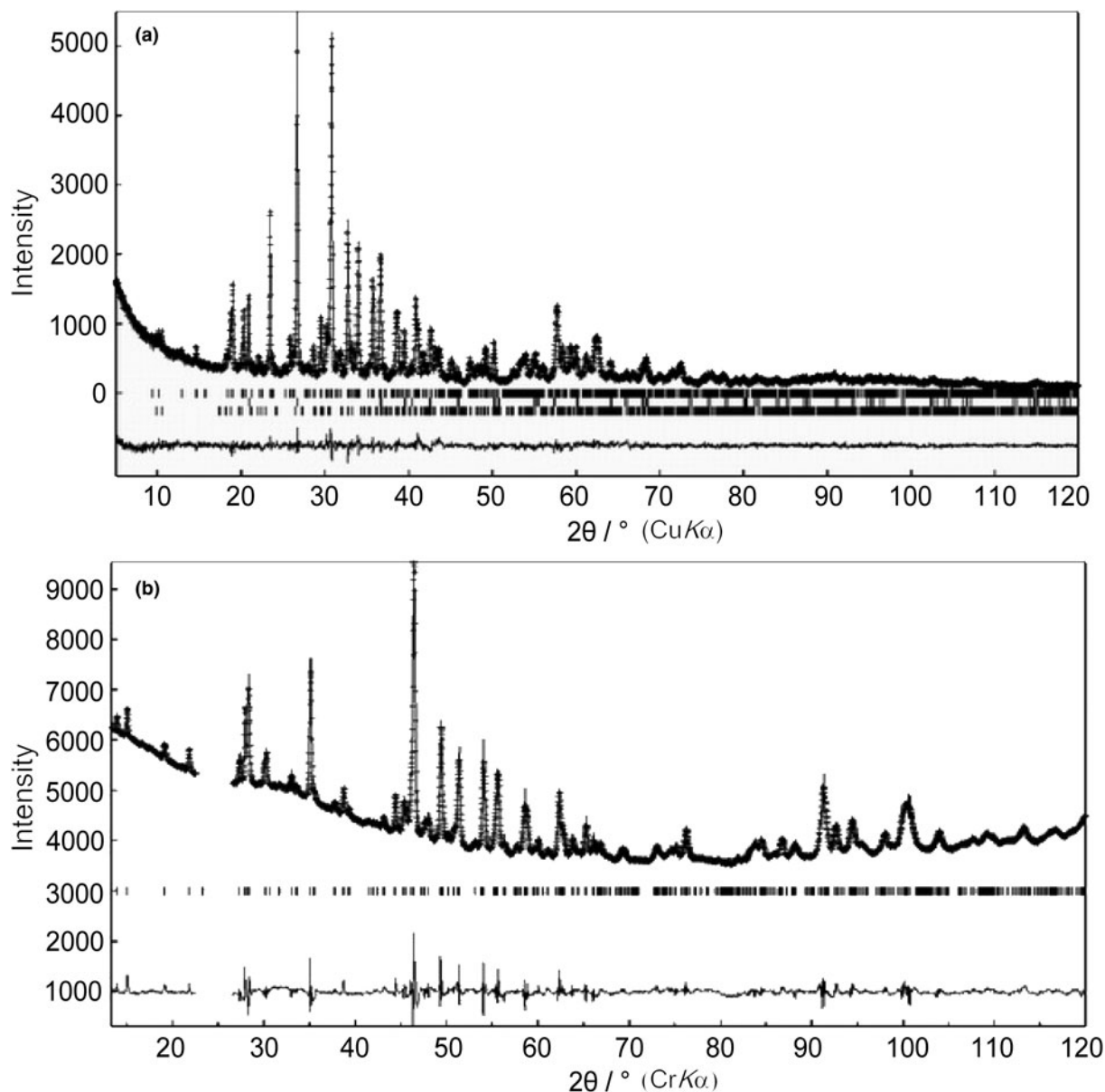


Figure 3. Observed and calculated powder X-ray diffraction patterns for the CLW (a) and CHG (b) pumpellyites. The CLW pumpellyite was refined with pumpellyite, quartz and hornblende, and the CHG pumpellyite with the single phase, pumpellyite. The crosses are the observed data, the solid line is the calculated pattern, and the vertical bars mark all possible Bragg reflections by $\text{CuK}\alpha$ and $\text{CrK}\alpha$ diffraction for CLW (a) and CHG (b), respectively. In the plot of CLW (a), the vertical bars of the top, middle, and bottom correspond to the Bragg reflections of pumpellyite, quartz and hornblende, respectively. The difference between the observed and calculated patterns is shown at the bottom.

mm/s for Fe^{2+} , we assigned the doublets CC' with I.S. = 0.11(2) and Q.S. = 0.29(4) mm/s, and DD' with I.S. = 1.17(2) and Q.S. = 2.74(2) mm/s to Fe^{3+} and Fe^{2+} in chlorite, respectively.

The $[\text{Fe}^{2+}(\text{X})]:[\text{Fe}^{3+}(\text{X}, \text{Y})]$ ratio in the CLW pumpellyite, determined from the area ratio of the doublets AA' and BB', is 15:85 in percent.

Discussion

Cation distribution in the X and Y sites of the CLW and CGH pumpellyites

By combining the refined site occupancies in the X and Y sites, $\text{Mg}_{0.298}\text{Fe}_{0.298(5)}\text{Al}_{0.405}$ and $\text{Fe}_{0.191}\text{Al}_{0.809}$, respectively

(Table 3), and the Ca, K, Na, Mn, V and Ti contents in the average chemical composition (Table 1), the empirical formula of the CLW pumpellyite is derived as follows: $(\text{Ca}_{7.96}\text{K}_{0.02}\text{Na}_{0.01})_{\Sigma 7.99}(\text{Mg}_{1.19}\text{Mn}_{0.09}\text{Fe}_{1.10}\text{Al}_{1.62})_{\Sigma 4.00}(\text{Al}_{6.47}\text{Fe}_{1.50}\text{V}_{0.02}\text{Ti}_{0.01})_{\Sigma 8.00}\text{Si}_{12.26}\text{O}_{56-n}(\text{OH})_n$. As the $\text{Fe}^{2+}:\text{Fe}^{3+}$ ratio of the CLW pumpellyite is $\text{Fe}^{2+}:\text{Fe}^{3+}=15:85$ in atomic percent, the structural formula is finally established as follows: $(\text{Ca}_{7.96}\text{K}_{0.02}\text{Na}_{0.01})_{\Sigma 7.99}(\text{Mg}_{1.19}\text{Mn}_{0.09}\text{Fe}_{0.39}\text{Fe}_{0.71}\text{Al}_{1.62})_{\Sigma 4.00}(\text{Al}_{6.47}\text{Fe}_{1.50}\text{V}_{0.02}\text{Ti}_{0.01})_{\Sigma 8.00}\text{Si}_{12.26}\text{O}_{43.33}(\text{OH})_{12.67}$.

In addition, the refined site occupancy of the CHG pumpellyite, $^{\text{X}}[\text{Mg}_{0.2435}\text{Fe}_{0.42(1)}\text{Al}_{0.34}]\text{Y}[\text{Fe}_{0.32}\text{Al}_{0.68}]$ (Table 3), and the EMPA data of the CHG pumpellyite (Table 1) result in the empirical formula of $(\text{Ca}_{8.01}\text{K}_{0.01})_{\Sigma 8.02}(\text{Mg}_{0.97}\text{Mn}_{0.02}\text{Fe}_{1.66}\text{Al}_{1.36})_{\Sigma 4.01}(\text{Al}_{5.44}\text{Fe}_{2.55}\text{V}_{0.01})_{\Sigma 8.00}\text{Si}_{12.02}\text{O}_{56-n}(\text{OH})_n$. Although

Table 3. Site occupancies (Occ.), atomic coordinates (x, y, z) and isotropic atomic displacement parameters (*B* in Å²) * of the CLW and CHG pumpellyites.

Site	Wyk*		CLW	CHG	Site	Wyk*		CLW	CHG
W1	4j	x	0.2529(4)	0.2546(9)	O1	8j	x	0.1371(9)	0.121(2)
		y	½	½			y	0.229(1)	0.241(4)
		z	0.3387(2)	0.3401(5)			z	0.0714(4)	0.0775(8)
		B	3.5(1)	0.43			B	3.5(1)	0.76
		Occ.	Ca1.0	Ca1.0			O2	8j	x
W2	4j	x	0.1907(5)	0.193(1)	y	0.236(1)	0.227(2)		
		y	½	½	z	0.2465(5)	0.249(1)		
		z	0.1533(2)	0.1543(5)	B	3.5	0.72		
		B	3.5	0.74	O3	8j	x		0.3638(9)
		Occ.	Ca1.0	Ca1.0	y		0.223(2)	0.219(3)	
X	4j	x	½	½	z		0.4166(4)	0.4151(8)	
		y	¼	¼	B		3.5	0.86	
		z	¼	¼	O4		4j	x	0.130(1)
		B	4.1(2)	0.67	y	½		½	
		Occ.	Mg0.298	Mg0.2435	z	0.4471(6)		0.447(2)	
	Fe0.298(5)	Fe0.42(1)	B	3.5	0.52				
	Al0.405	Al0.34	O5	4j	x	0.139(1)		0.126(3)	
Y	8j	x	0.2527(6)		0.2628(8)	y	0	0	
		y	0.256(1)		0.250(2)	z	0.4555(6)	0.463(2)	
		z	0.4964(3)		0.4960(5)	B	3.5	1.06	
		B	4.1		0.48	O6	4j	x	0.370(1)
		Occ.	Fe0.191	Fe0.32	y	½		½	
	Al0.809	Al0.68	z	0.0534(6)	0.048(1)				
	0.0525(8)	0.055(1)	B	3.5	0.55				
	0	0	O7	4j	x	0.372(1)		0.376(3)	
Si1	4j	z	0.0918(4)		0.0924(8)	y	0	0	
		B	4.1(2)		0.33	z	0.0350(7)	0.033(1)	
			0.1692(7)		0.165(1)	B	3.5	1.07	
			0		0	O8	4j	x	0.038(1)
			0.2498(3)	0.2489(7)	y	0		0	
	3.5(2)	0.41	z	0.1789(5)	0.180(1)				
	0.4589(9)	0.460(2)	B	3.5	0.79				
	0	0	O9	4j	x	0.479(1)		0.475(2)	
Si2	4j	z	0.4011(4)		0.4029(7)	y	1/2	1/2	
		B	4.3(2)		0.30	z	0.1752(5)	0.178(1)	
						B	3.5	0.56	
						O10	4j	x	0.068(1)
					y	0		0	
			z	0.3182(5)	0.322(2)				
			B	3.5	1.04				
			O11	4j	x	0.505(1)		0.520(2)	
			y		1/2	1/2			
			z		0.3143(6)	0.314(1)			
			B		3.5	0.93			

Notes: On the basis of the chemical composition data, the site occupancies of Ca at the W1 and W2 sites and of Si at the Si1, Si2 and Si3 sites were fixed to 1.0, and that of Mg at the X site was fixed to the chemical composition value. The site occupancies of Al and Fe in the X and Y sites were refined using the following constraints: Al(X) = 1.0 - Mg(X) - Fe(X); Fe(Y) = [total Fe apfu - 4×Fe(X)]/8; and Al(Y) = 1.0 - Fe(Y). Estimated standard deviations are in parentheses (1σ). The isotropic atomic displacement parameters of the CLW pumpellyite were refined using the constraints B(W2) = B(W1); B(Y) = B(X); and B(O2) to B(O11) = B(O1), whereas those of the CHG pumpellyite were fixed to those of julgöldite determined by Allmann and Donnay (1973). * Wyk is Wyckoff site notation.

the Fe²⁺:Fe³⁺ ratio in the CHG pumpellyite was not determined in the present study, we assume that the oxidation state of Fe in the CHG pumpellyite is almost the same as that of the CLW pumpellyite, because the green rock samples of the CLW and CHG pumpellyites are from the same outcrop and their mineral assemblages and the occurrence of metamorphic minerals are similar to each other. By applying the Fe²⁺:Fe³⁺ ratio of the CLW pumpellyite (i.e. Fe²⁺:Fe³⁺ = 15:85) to the CHG pumpellyite, the empirical formula of the CHG pumpellyite becomes (Ca_{8.01}K_{0.01})_{Σ8.02}(Mg_{0.97}Mn_{0.02}Fe_{0.63}²⁺Fe_{1.03}³⁺Al_{1.36})_{Σ4.01}(Al_{5.44}Fe_{2.55}³⁺V_{0.01})_{Σ8.00}Si_{12.02}O_{42.69}(OH)_{13.31}.

The consistency between the determined site populations and the structural characteristics can be examined using the bond-valence-sum rule (Brown and Shannon, 1973): $V_i = \sum_j \exp[(l_0 - l_{ij})/0.37]$, where V_i is the valence or oxidation state of cation i , l_0 is the bond-valence parameter (Brown and

Altermatt 1985; Brese and O'Keeffe 1991) and l_{ij} is the bond length between cation i and anion j (Table 7). The bond-valence sums of the W1, W2, Y and tetrahedral Si1, Si2 and Si3 sites of the CLW pumpellyite are close to the expected values, and that of the X site, 2.36 in valence units, is consistent with the presence of both divalent and trivalent cations in this site. Thus, the resulting bond-valence sums of the cation sites imply that the determined site populations for the CLW pumpellyite are reasonable. On the other hand, the bond-valence sums of the CHG pumpellyite deviate somewhat from the expected value: the valence sums of the W2, Y, Si1, Si2 and Si3 sites are 2.23, 2.82, 3.87, 4.27 and 3.81 in valence units, respectively, versus the expected values of 2, 3, 4, 4 and 4 vu, respectively. A reason could be attributed to the somewhat low X-ray diffraction intensity data due to a very small quantity of the CHG sample. However, the deviation of the bond-valence sums of the cation sites from the expected

Table 4. Selected bond lengths (Å).

	CLW	CHG		CLW	CHG		CLW	CHG
W1-O2 ×2	2.368(9)	2.381(17)	X-O2 ×2	2.138(9)	2.230(17)	Si1-O1 ×2	1.627(9)	1.59(3)
W1-O3 ×2	2.350(9)	2.329(17)	X-O9 ×2	2.056(8)	2.025(19)	Si1-O4	1.688(11)	1.69(3)
W1-O4	2.465(11)	2.467(29)	X-O11 ×2	1.926(8)	1.925(18)	Si1-O8	1.690(12)	1.70(3)
W1-O8	2.556(12)	2.606(21)	Mean <X-O>	2.040	2.06	Mean <Si1-O>	1.66	1.64
W1-O11	2.337(11)	2.468(21)	Y-O1	1.870(9)	2.132(15)	Si2-O2 ×2	1.608(8)	1.544(15)
Mean <W1-O>	2.40	2.42	Y-O3	1.932(9)	1.889(16)	Si2-O8	1.665(11)	1.60(3)
W2-O1 ×2	2.254(9)	2.172(18)	Y-O4	1.978(9)	2.07(2)	Si2-O10	1.679(11)	1.73(3)
W2-O2 ×2	2.394(9)	2.440(17)	Y-O5	1.930(9)	1.970(19)	Mean <Si2-O>	1.64	1.61
W2-O6	2.641(11)	2.687(26)	Y-O6	2.069(10)	1.93(2)	Si3-O3 ×2	1.616(10)	1.600(19)
W2-O9	2.530(12)	2.486(21)	Y-O7	1.887(9)	1.881(19)	Si3-O6	1.644(13)	1.74(3)
W2-O10	2.423(10)	2.420(22)	Mean <Y-O>	1.944	1.98	Si3-O9	1.627(12)	1.72(3)
Mean <W2-O>	2.413	2.40				Mean <Si3-O>	1.63	1.67

Table 5. Bond angle variance $\sigma_0(\text{oct})^2$ (degree²), quadratic elongation $\langle\lambda_{\text{oct}}\rangle$, and bond-length distortion index DI^* of XO_6 octahedra versus $\text{Fe}^{2+} + \text{Fe}^{3+}$ in the X site and those of YO_6 octahedra versus Fe^{3+} in the Y site.

Pumpellyite	X site				Y site			
	$^X[\text{Fe}^{2+} + \text{Fe}^{3+}]$	$\sigma_0(\text{oct})^2$	$\langle\lambda_{\text{oct}}\rangle$	DI	$^Y[\text{Fe}^{3+}]$	$\sigma_0(\text{oct})^2$	$\langle\lambda_{\text{oct}}\rangle$	DI
CLW	1.10	16.98	1.009	0.037	1.53	36.32	1.013	0.027
CHG	1.66	28.02	1.015	0.055	2.33	55.02	1.018	0.041

* Bond angle variance and quadratic elongation are defined by Robinson *et al.* (1971), and bond-length distortion index by Baur (1974). The definitions are given in the text.

values is not serious, and, as a whole, the chemical and structural data of the CHG pumpellyite are regarded to have an adequate quality to supply useful information on the Fe^{2+} and Fe^{3+} distributions in the X and Y sites and their effects on the structure. The sums of O5, O7 and O10 are close to 1.0 which is the expected value for a hydroxyl group, implying the existence of $(\text{OH})^-$ at these oxygen positions, as has been clarified repeatedly by the structural analyses of the pumpellyite structure (e.g. Allmann and Donnay, 1971, 1973; Yoshiasa and Matsumoto, 1985, Nagashima *et al.*, 2006). The valence sums for O11 of the CLW and CHG pumpellyites, 1.36 and 1.31, respectively, are rather larger than the expected value for a hydroxyl group as well as the published data (e.g. Allmann and Donnay, 1971, 1973; Yoshiasa and Matsumoto, 1985, Nagashima *et al.*, 2006). Such deviation of the O11 valence sum from the expected value for a hydroxyl group has been explained by charge equalisation between $\text{O}(10)^{2-}$ and $\text{O}(10)\text{H}^-$ and $\text{O}(11)^{2-}$ and $\text{O}(11)\text{H}^-$ (Allmann and Donnay, 1971) and by reduction of the number of hydrogen atoms at the X site by a possible substitution of $[\text{M}^{3+}(\text{X}) + \text{O}^{2-}(\text{O11})]$ for $[\text{M}^{2+}(\text{X}) + \text{H}^+(\text{H11}) + \text{O}^{2-}(\text{O11})]$ (Yoshiasa and Matsumoto, 1985). Both interpretations seem to be adequate for understanding the valence sums of O11 of the CLW and CHG pumpellyites.

To conclude, the self-consistency between the determined site populations and the measured bond lengths of the CLW and CHG pumpellyites is proved using the bond-valence-sum rule. The established structural formulae indicate that the proper name of the CLW and CHG pumpellyites is pumpellyite-(Al). Hereafter, the numbers of cations at the X and Y sites shown in the given structural formula are referred to as the site populations at the X and Y sites in the CLW and CHG pumpellyites.

Change of cation populations in the X and Y sites with increasing total Fe in pumpellyite

The constructed structural formulae of the CLW and CHG pumpellyites indicate the nonselective distribution of Fe^{3+} and Al in the X and Y sites, as well as the results of the published studies for Fe-rich pumpellyites cited already. Systematic variation of the Fe distribution in the X and Y sites can be elucidated from the results of the present study and the published data listed in Table 8, where the data for juldolites are also shown for comparison.

The data show that Fe in the X and Y sites, ^XFe and ^YFe , respectively, increase linearly versus the total Fe content (Fig. 5) as shown by the following regression equations:

$$^X\text{Fe apfu} = 0.3084 \times [\text{total Fe}]^{\text{pumpellyite}} + 0.2815 \quad (R^2 = 0.66), \text{ and} \quad (1)$$

$$^Y\text{Fe apfu} = 0.7485 \times [\text{total Fe}]^{\text{pumpellyite}} - 0.4336 \quad (R^2 = 0.93). \quad (2)$$

The ^XFe and ^YFe correspond to $\text{Fe}^{2+} + \text{Fe}^{3+}$ in the X site and Fe^{3+} in the Y site, respectively. In the Y site, Fe^{3+} substitutes for Al^{3+} or is incorporated instead of Al^{3+} , as has been repeatedly confirmed to date (e.g. Artioli and Geiger, 1994; Akasaka *et al.*, 1997; Nagashima *et al.*, 2006). On the contrary, the increase of Fe at the X site is related to the decrease of Mg^{2+} and Al^{3+} (Fig. 6):

$$^X\text{Mg}^{2+}(\text{apfu}) = -0.5187 \times ^X\text{Fe}(\text{apfu}) + 1.726 \quad (R^2 = 0.85), \quad (3)$$

$$^X\text{Al}^{3+}(\text{apfu}) = -0.4949 \times ^X\text{Fe} + 2.2898 \quad (R^2 = 0.78), \quad (4)$$

$$^X\text{Fe}^{3+}(\text{apfu}) = 0.8018 \times ^X\text{Fe} - 0.425 \quad (R^2 = 0.85) \text{ and} \quad (5)$$

$$^X\text{Fe}^{2+}(\text{apfu}) = 0.1800 \times ^X\text{Fe} + 0.4782 \quad (R^2 = 0.16). \quad (6)$$

The decreasing rates of Mg and Al with the increase of Fe at the X site are almost the same (equations 3 and 4). The higher

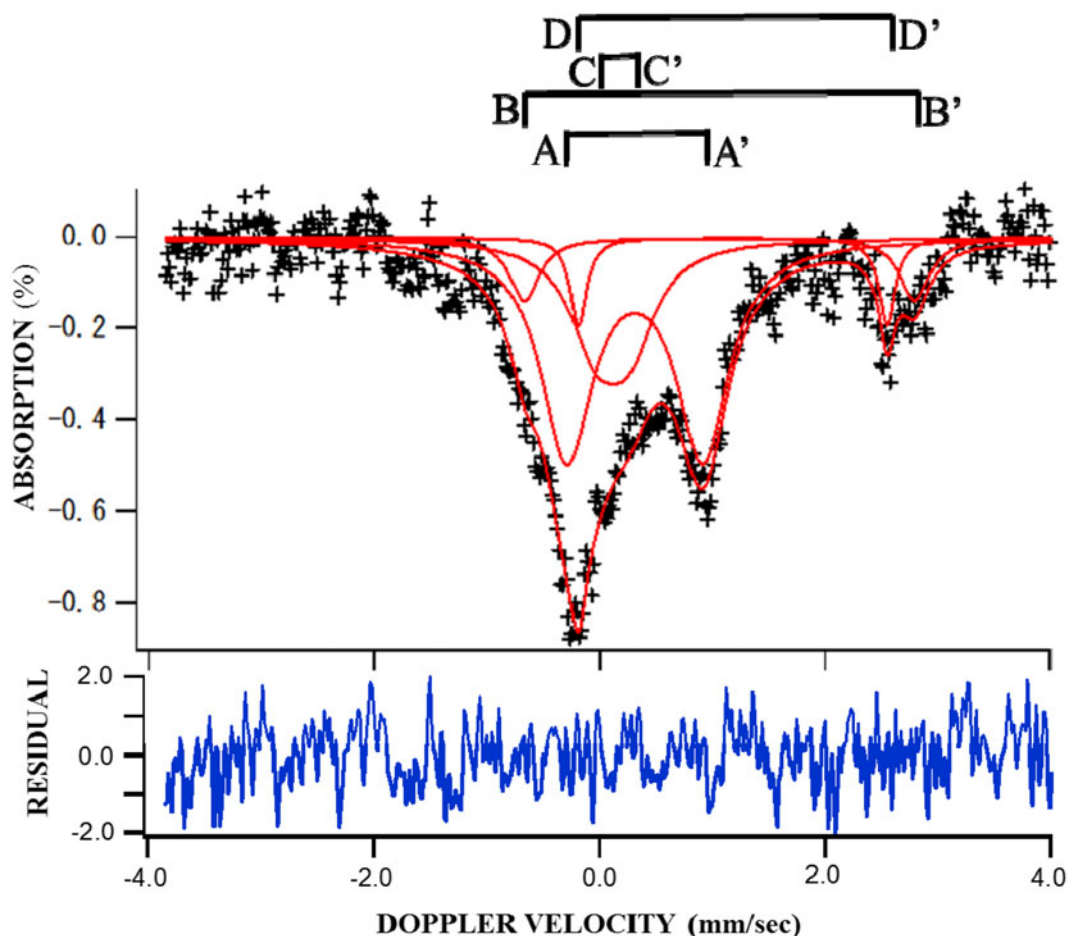


Figure 4. ⁵⁷Fe Mössbauer spectrum of the CLW pumpellyite and the fitted data. Mössbauer hyperfine parameters and the assignments are shown in Table 6.

Table 6. ⁵⁷Fe Mössbauer hyperfine parameters of the doublets in ⁵⁷Fe Mössbauer spectrum of the CLW pumpellyite sample*.

Doublets	I.S. (mm/s)	Q.S. (mm/s)	Γ (mm/s)	Area ratio (%)	Assignment
AA'	0.31(1)	1.21(2)	0.56(2)	58(4)	Fe ³⁺ (X, Y) in pumpellyite
BB'	1.06(2)	3.46(4)	0.32(7)	10(2)	Fe ²⁺ (X) in pumpellyite
CC'	0.11(2)	0.29(4)	0.56(7)	25(2)	Fe ³⁺ in chlorite
DD'	1.17(2)	2.74(2)	0.18(3)	7(2)	Fe ²⁺ in chlorite

* Estimated standard deviations are in parentheses (1σ). I.S. = isomer shift relative to metallic absorber (mm/s), Q.S. = quadrupole splitting (mm/s), Γ = full width at half height (mm/s).

rate of increase of Fe³⁺, 0.8018^XFe³⁺ (apfu) per ^XFe, and the lower rate of increase of Fe²⁺, 0.1800^XFe²⁺ per ^XFe, with increasing total Fe on the X site indicates that Fe³⁺ compensates for not only the decrease of Al but also the decrease of Mg, and that the contribution of the substitution Mg²⁺ + Al³⁺ ↔ Fe²⁺ + Fe³⁺ is rather limited. This result implies that the increase of Fe³⁺ over Fe²⁺ at the X site is a characteristic crystallochemical feature of Fe-rich pumpellyites in low-grade metamorphic rocks with zeolite to prehnite–pumpellyite facies or hydrothermally altered igneous rocks under high oxygen-fugacity conditions. At temperatures of zeolite-facies metamorphism where epidote cannot coexist

with pumpellyite, Fe³⁺ concentrates in pumpellyite, whereas aluminous pumpellyites occurring in metamorphic rocks of the higher grade pumpellyite–actinolite facies are low in Fe³⁺ and high in Fe²⁺ contents (e.g. Coombs *et al.*, 1976), because of Fe³⁺ concentration in epidote coexisting with pumpellyite (Schiffman and Liou, 1983). Thus, the increase in Fe³⁺ at the X site over Fe²⁺ in Fe-rich pumpellyite, including the CLW and CHG pumpellyites, can be attributed to the high Fe³⁺ content in the bulk composition of the host rocks and non-coexistence of pumpellyite with epidote.

The preference of the trivalent transition metal cation (M³⁺) versus Al³⁺ in the X and Y sites is evaluated using the distribution coefficient $K_D = (M^{3+}/Al^{3+})^X / (M^{3+}/Al^{3+})^Y$ (Nagashima and Akasaka, 2007; Nagashima *et al.*, 2010; Hamada *et al.*, 2010), and, thus, the distribution coefficient $K_D = (Fe^{3+}/Al^{3+})^X / (Fe^{3+}/Al^{3+})^Y$ for the distribution of Fe³⁺ and Al³⁺ in the X and Y sites can be applied to Fe-rich pumpellyites. The K_D values of the CLW and CGH pumpellyites calculated using the determined site populations (Table 8) are 1.62 and 1.90, respectively, indicating a stronger preference for Fe³⁺ than Al³⁺ in the X site. Our results are consistent with the K_D values of 1.44 and 1.12 for Fe-rich pumpellyites with 2.40 and 3.99 apfu total Fe, respectively, reported by Nagashima *et al.* (2006).

As Nagashima *et al.* (2010) pointed out, Cr³⁺ ions with a smaller ionic radius than Fe³⁺ prefer the X site with a larger octahedral volume than the Y site, which is also proved by K_D values, defined as $(Cr/Al)^X / (Cr/Al)^Y$, of 3.56 and 4.39 after Nagashima and

Table 7. Bond valences (V) in valence unit and cationic and anionic bond valence sums ($\Sigma_C V$ and $\Sigma_A V$, respectively) of the CLW and CHG pumpellyites.

CLW	Cations									
	W1	W2	X	Y	Si1	Si2	Si3	$\Sigma_C V$	Anion chemistry	
Anions										
O1		^{×21} 0.42		0.59	^{×21} 1.04			2.05		O ²⁻
O2	^{×21} 0.32	^{×21} 0.30	^{×21} 0.30			^{×21} 1.09		2.01		O ²⁻
O3	^{×21} 0.33			0.50			^{×21} 1.07	1.90		O ²⁻
O4	0.25			0.44 ^{×2→}	0.88			2.01		O ²⁻
O5				0.50 ^{×2→}				1.00		OH ⁻
O6		0.16		0.36 ^{×2→}			0.99	1.87		O ²⁻
O7				0.57 ^{×2→}				1.14		OH ²⁻
O8	0.20				0.87	0.94		2.01		O ²⁻
O9		0.21	^{×21} 0.37 ^{×2→}				1.03	1.98		O ²⁻
O10		0.28				0.90		1.18		OH ⁻
O11	0.34		^{×21} 0.51 ^{×2→}					1.36		OH ⁻
$\Sigma_A V$	2.09	2.09	2.36	2.96	3.83	4.02	4.16			
CHG	Cations									
	W1	W2	X	Y	Si1	Si2	Si3	$\Sigma_C V$	Anion chemistry	
Anions										
O1		^{×21} 0.51		0.30	^{×21} 1.10			1.91		O ²⁻
O2	^{×21} 0.31	^{×21} 0.27	^{×21} 0.24			^{×21} 1.23		2.05		O ²⁻
O3	^{×21} 0.35			0.58			^{×21} 1.11	2.04		O ²⁻
O4	0.25			0.36 ^{×2→}	0.85			1.82		O ²⁻
O5				0.47 ^{×2→}				0.94		OH ⁻
O6		0.15		0.52 ^{×2→}			0.78	1.97		O ²⁻
O7				0.59 ^{×2→}				1.18		OH ⁻
O8	0.18				0.82	1.06		2.06		O ²⁻
O9		0.24	^{×21} 0.41 ^{×2→}				0.81	1.87		O ²⁻
O10		0.28				0.75		1.03		OH ⁻
O11	0.25		^{×21} 0.53 ^{×2→}					1.31		OH ⁻
$\Sigma_A V$	2.00	2.23	2.36	2.82	3.87	4.27	3.81			

Superscripts left and right of the bond valences indicate number of bonds per cation and anion, respectively.

Table 8. Site population data and bond lengths for pumpellyite–julgoldite-series minerals, from this study and literature.

Specimen	Total Fe (apfu)	$X[\text{Fe}^{2+}+\text{Fe}^{3+}]$ (apfu)	$\langle X-O \rangle$ (Å)	Cation population in the X site (apfu)					$Y\text{Fe}^{3+}$ (apfu)	$\langle Y-O \rangle$ (Å)	References
				Mg ²⁺	Mn ²⁺	Fe ²⁺	Fe ³⁺	Al ³⁺			
Pumpellyite CLW from Chichibu	2.60	1.10	2.040	1.19	0.09	0.39	0.71	1.62	1.50	1.944	This study
Pumpellyite CHG from Chichibu	4.21	1.66	2.06	0.97	0.02	0.63	1.03	1.36	2.55	1.98	This study
Pumpellyite MTS from Shimane	3.99	1.65	2.053	0.68	-	0.88	0.77	1.66	2.34	1.943	Nagashima <i>et al.</i> (2006)
Pumpellyite KGH from Shimane	2.40	1.11	2.031	1.24	-	0.65	0.46	1.66	1.29	1.943	Nagashima <i>et al.</i> (2006)
Pumpellyite from Gumma	0.92	0.92	2.008	1.34	-	0.92*		1.86	0.00	1.918	Yoshiasa and Matsumoto (1985)
Pumpellyite HR from Hicks Ranch	0.95	0.95	1.99	1.20	-	0.77	0.18	1.85	0.00	1.920	Galli and Alberti (1969)
Pumpellyite HR from Hicks Ranch	0.77	0.50	1.993	1.40	-	0.50	0.00	2.20	0.27	1.935	Artioli and Geiger (1994)
Pumpellyite K1 from Keweenaw	1.44	0.40	1.986	1.50	-	0.40	0.00	2.00	1.04	1.947	Artioli and Geiger (1994)
Pumpellyite BU from Torrente Bulla	3.35	0.80	2.027	1.30	-	0.80	0.00	1.90	2.55	1.948	Artioli and Geiger (1994)
Julgoldite from Långban	11.10	3.90	-	0.10	-	2.70	1.20	-	7.20	-	Moore (1971)
Julgoldite from Långban	11.50	4.00	2.084	0.00	-	2.00	2.00	0.00	7.50	2.011	Allmann and Donnay (1973)
Julgoldite from Kilsyth	11.56	3.88	-	0.12	-	3.00	0.88	0.00	7.68	-	Livingstone (1976)
Julgoldite-(Fe ³⁺) from Bombay	10.69	2.70	2.079	0.20	-	0.00	2.70	1.10	7.99	2.048	Artioli <i>et al.</i> (2003)
Julgoldite-(Fe ²⁺) from Bombay	9.76	2.88	2.062	0.68	-	1.76	1.16	0.40	6.88	2.00	Nagashima <i>et al.</i> (2018)
Julgoldite-(Fe ²⁺) from Kreimbach/Kaulbach	9.16	2.68	2.062	0.64	-	2.68*		0.68	6.48	2.01	Nagashima <i>et al.</i> (2018)
Julgoldite-(Fe ³⁺) from Crimea	11.56	3.60	2.08	0.20	0.04	1.12	2.48	0.00	7.96	2.01	Kasatkin <i>et al.</i> (2021)

* Total Fe as Fe²⁺.

Akasaka (2007) and of 1.66–4.54 by Hamada *et al.* (2010). The reason for different K_D values of Fe³⁺ and Cr³⁺ compared to Al³⁺ has not been explained previously. Hamada *et al.* (2010) noted that the K_D values of Cr³⁺ versus Al tend to increase with increasing Cr content in pumpellyite, however the possible dependence of the K_D values of Fe³⁺ versus Al on the Fe content in pumpellyite has not been described previously.

Dependence of structural properties on Fe content at the X and Y sites

As shown by the studies cited above, the influence of total Fe in the pumpellyite and Fe population at the X and Y sites on the pumpellyite structure has been well described using the bond lengths at the octahedral sites and the unit-cell parameters.

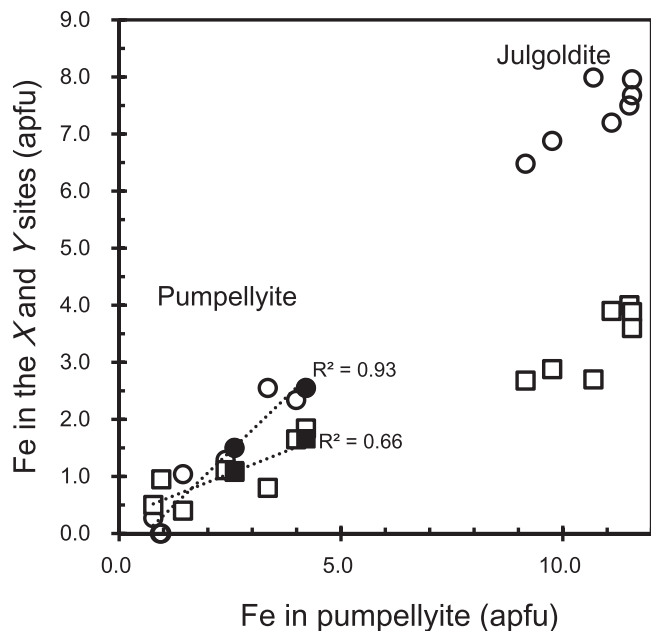


Figure 5. Fe content (apfu) in the X and Y sites versus total Fe (apfu) in pumpellyite and juldolite. Closed circle: Fe³⁺ in the Y site of the CLW and CHG pumpellyites in this study; open circle: Fe³⁺ in the Y site of pumpellyite and juldolite listed in Table 8; closed square: total Fe in the X site of the CLW and CHG pumpellyites in this study; open square: total Fe in the X site of pumpellyite and juldolite listed in Table 8. To avoid complexity, each data source other than this study is not distinguished. The dotted lines are regression lines of equations (1) with R²=0.66 and (2) with R²=0.93, shown in the document.

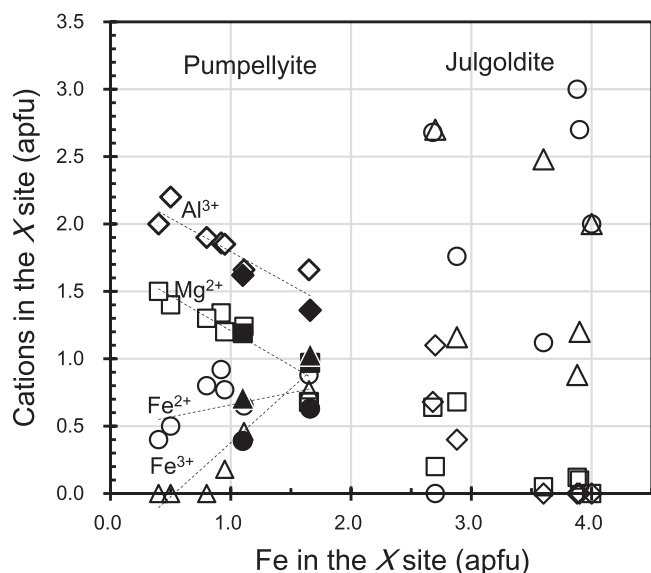


Figure 6. Mg²⁺, Fe²⁺, Fe³⁺ and Al³⁺ contents versus total Fe in the X site. Square: Mg²⁺, circle: Fe²⁺, triangle: Fe³⁺, diamond: Al³⁺. Closed marks are of CLW and CHG pumpellyites with XFe = 1.10 and 1.66 apfu, respectively, and open marks of the published pumpellyites and juldolites. Data sources are listed in Table 8. Dashed lines are regression lines of X[Mg²⁺], X[Al³⁺], X[Fe³⁺] and X[Fe²⁺], represented by equations 3–6, respectively, in the document.

The mean <Y–O> distances of the CLW and CHG pumpellyites together with other Fe-bearing pumpellyites (Table 8) show an increase of the mean <Y–O> distance versus Fe³⁺ in the Y site (Fig. 7b):

$$\begin{aligned} \text{Mean } \langle Y-O \rangle \text{ distance } (\text{\AA}) \\ = 0.014 \times Y \text{Fe}^{3+}(\text{apfu}) + 1.9241 \quad (R^2 = 0.65). \end{aligned} \quad (7)$$

The linear variation of the mean <Y–O> distance versus Fe³⁺ in the Y site has been shown previously by Nagashima *et al.* (2006) in which, instead of Fe³⁺ content in the Y site, the average ionic radius at the Y site is employed. In addition, the mean <X–O> distances of the CLW and CHG pumpellyites and published Fe-bearing pumpellyites (Table 8) show that the mean <X–O> distance increases with increasing total Fe content at the X site (Fig. 7a):

$$\begin{aligned} \text{Mean } \langle X-O \rangle \text{ distance } (\text{\AA}) \\ = 0.056 \times X[\text{Fe}^{2+} + \text{Fe}^{3+}](\text{apfu}) \\ + 1.9644 \quad (R^2 = 0.78). \end{aligned} \quad (8)$$

The mean <X–O> distance per X[Fe²⁺ + Fe³⁺] apfu [0.056 Å] is larger than that of the mean <Y–O> distance per YFe³⁺ [0.0128 Å], which suggests that the simultaneous substitutions of Fe²⁺ for Mg²⁺ and of Fe³⁺ for Al³⁺ significantly affect the increase of the mean <X–O> distance.

The changes in the mean <X–O> and <Y–O> distances versus Fe content in the X and Y sites correspond to the volumetric change of the XO₆ and YO₆ octahedra, and result in the change in distortion of XO₆ and YO₆ octahedra. The YO₆ octahedra are geometrically more distorted than the centrosymmetric XO₆ octahedra (Galli and Alberti, 1969; Yoshiasa and Matsumoto, 1985). Artioli and Geiger (1994) and Akasaka *et al.* (1997) confirmed stronger Y-site distortion than the X site by applying the quadratic elongation <λ_{oct}> and bond-angle variance σ_θ(oct)²: X[<λ_{oct}>] < Y[<λ_{oct}>] and X[σ_θ(oct)²] < Y[σ_θ(oct)²] (Table 9; Fig. 8). However, the combined X-ray diffraction and ⁵⁷Fe Mössbauer spectroscopic studies by Artioli *et al.* (2003) and Nagashima *et al.* (2006) showed that Q.S. values of the Mössbauer doublets assigned to Fe³⁺ at the X site are larger than those of the doublets by Fe³⁺ at the Y site, which implies the stronger distortion of the XO₆ octahedra than the YO₆ octahedra. In addition, Nagashima *et al.* (2006) found that, in contrast to the site distortion represented by the quadratic elongation <λ_{oct}>, the bond-length distortion index DI(oct) of the XO₆ octahedra is larger than that of the YO₆ octahedra (Table 9; Fig. 8), and, thus, the DI(oct) is consistent with the site distortion of the XO₆ octahedra identified from the Mössbauer spectroscopic analysis. As shown in Table 9 and Fig. 8, the σ_θ(oct)², <λ_{oct}> and DI(oct) for the Fe content in the Y site of the CLW pumpellyite are all in harmony with those reported for pumpellyites, and tend to decrease with increasing Fe content in the Y site. The σ_θ(oct)², <λ_{oct}> and DI(oct) at the X site of the CLW pumpellyite are also similar to those of the published pumpellyites. Although a dependence of X[<λ_{oct}>] on Fe content in the X site is not observed, X[σ_θ(oct)²] and X[DI(oct)] show a weak decrease and an increase versus Fe content in the X site, respectively. Whereas the σ_θ(oct)², <λ_{oct}> and DI(oct) at the X and Y sites in the CHG pumpellyite are significantly larger than those of the CLW and published pumpellyites. Its reason may be attributed to rather poor X-ray diffraction intensity data obtained from a small quantity of the CHG sample, as mentioned in the discussion for the valence sums of the CGH pumpellyite (Table 7). Despite this problem, the relationships X[<λ_{oct}>] < Y[<λ_{oct}>], X[σ_θ(oct)²] < Y[σ_θ(oct)²], and X[DI] > Y[DI]

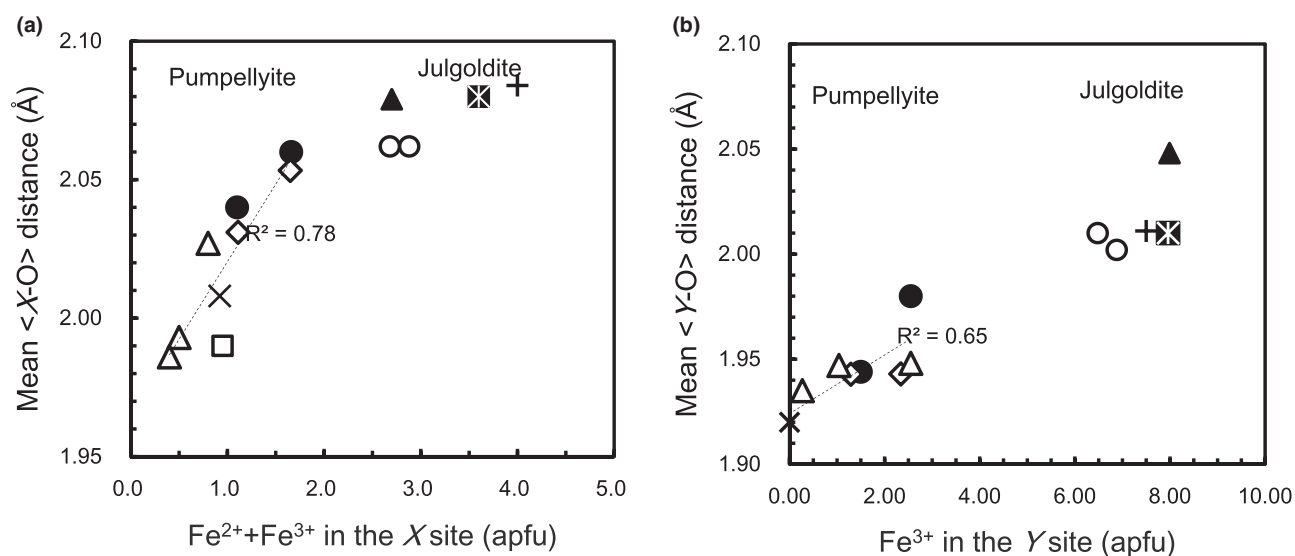


Figure 7. (a) Variation of mean $\langle X-O \rangle$ distance with $X[\text{Fe}^{2+}+\text{Fe}^{3+}]$ and (b) mean $\langle Y-O \rangle$ distance with $Y\text{Fe}^{3+}$ of pumpellyite and julgoldite listed in Table 8. Closed circle: CLW and CGH pumpellyites in this study; open diamond: Nagashima *et al.* (2006); multiplication sign: Yoshiasa and Matsumoto (1985); open square: Galli and Alberti (1969); open triangle: Artioli and Geiger (1994); plus sign: Allmann and Donnay (1973); closed triangle: Artioli *et al.* (2003); open circle: Nagashima *et al.* (2018); closed star: Kasatkin *et al.* (2021). Dashed lines in (a) and (b) are regression lines represented by equations 8 and 7, respectively, in the document.

Table 9. X-site distortion versus $\text{Fe}^{2+}+\text{Fe}^{3+}$ in the X-site and Y-site distortion versus Fe^{3+} in the Y site in pumpellyite and julgoldite.*

Species	X site				Y site				References
	$X[\text{Fe}^{2+}+\text{Fe}^{3+}]$	$\sigma_{\theta}(\text{oct})^2$	$\langle \lambda_{\text{oct}} \rangle$	DI	$Y[\text{Fe}^{3+}]$	$\sigma_{\theta}(\text{oct})^2$	$\langle \lambda_{\text{oct}} \rangle$	DI	
Pumpellyite CLW from Chichibu	1.10	16.98	1.009	0.037	1.53	36.32	1.013	0.027	This study
Pumpellyite CHG from Chichibu	1.66	28.02	1.015	0.055	2.33	55.02	1.018	0.041	This study
Pumpellyite MTS from Shimane	1.65	14.41	1.007	0.034	2.34	36.39	1.012	0.021	Nagashima <i>et al.</i> (2006)
Pumpellyite KGH from Shimane	1.11	18.41	1.008	0.035	1.29	35.25	1.011	0.022	Nagashima <i>et al.</i> (2006)
Pumpellyite from Gumma	0.92	16.83	1.007	0.028	0.00	37.46	1.012	0.022	Yoshiasa and Matsumoto (1985)
Pumpellyite HR from Hicks Ranch	0.95	21.08	1.008	0.030	0.00	31.63	1.011	0.026	Galli and Alberti (1969)
Pumpellyite HR from Hicks Ranch	0.50	18.20	1.006	0.011	0.30	28.39	1.009	0.018	Artioli and Geiger (1994)
Pumpellyite K1 from Keweenaw	0.40	26.64	1.010	0.030	1.10	34.01	1.010	0.022	Artioli and Geiger (1994)
Pumpellyite BU from Torrente Bulla	0.80	19.79	1.008	0.027	2.60	30.16	1.009	0.019	Artioli and Geiger (1994)
Julgoldite from Långban	4.00	14.55	1.006	0.029	8.00	29.59	1.009	0.014	Allmann and Donnay (1973)
Julgoldite-(Fe^{3+}) from Bombay	2.70	5.98	1.002	0.018	8.00	16.30	1.005	0.012	Artioli <i>et al.</i> (2003)
Julgoldite-(Fe^{2+}) from Bombay	2.88	17.81	1.007	0.029	6.56	28.45	1.009	0.015	Nagashima <i>et al.</i> (2018)
Julgoldite-(Fe^{2+}) from Kreimbach/Kaulbach	2.68	15.21	1.007	0.031	6.48	26.22	1.008	0.014	Nagashima <i>et al.</i> (2018)
Julgoldite-(Fe^{3+}) from Crimea	3.60	12.36	1.004	0.017	7.96	27.92	1.008	0.014	Kasatkin <i>et al.</i> (2021)

*Notes: $\sigma_{\theta}(\text{oct})^2$ and $\langle \lambda_{\text{oct}} \rangle$ are angular and bond-length distortion indices by Robinson *et al.* (1971), respectively; DI is distortion index by Baur (1974).

and the contradictory relationship for site distortion between $\langle \lambda_{\text{oct}} \rangle$ and DI are also the case in the CGH pumpellyite (Table 9; Fig. 8), and, thus, are consistent with those of the CLW pumpellyite and the reported Fe-bearing pumpellyites. As concluded by Nagashima *et al.* (2006), the bond-length distortion index, DI(oct), of pumpellyite agrees with the distortion of the octahedral sites inferred by Mössbauer spectroscopy.

The *a*-, *b*-, and *c*-dimensions and cell volumes of the CLW and CGH pumpellyites are consistent with those of published pumpellyites (Table 10 and Fig. 9). The β angles of the CLW and CHG pumpellyites are also in harmony with those of the published pumpellyites, except for the data for the Hicks Ranch pumpellyite by Galli and Alberti (1969) and of Tokoro and Mitsu pumpellyites by Akasaka *et al.* (1997). However, according to the new unit-cell parameters of the Hicks Ranch and Mitsu pumpellyites obtained using the X-ray Rietveld refinement by Artioli

and Geiger (1994) and Nagashima *et al.* (2006), respectively, the β angles of the Hicks Ranch and the Mitsu pumpellyites are $97.433(2)^\circ$ and $97.462(1)^\circ$, respectively, and agree with the values of the CLW and CHG pumpellyites and other published pumpellyites (Table 10; Fig. 9).

The regression lines of the unit-cell parameters and the cell volume versus total Fe (Fig. 9) in the present study and published data listed in Table 10 are:

$$a \text{ (\AA)} = 0.0112 \times [\text{Total Fe (apfu)}] + 8.8089 \quad (R^2 = 0.78), \quad (9)$$

$$b \text{ (\AA)} = 0.0154 \times [\text{Total Fe (apfu)}] + 5.8923 \quad (R^2 = 0.83), \quad (10)$$

$$c \text{ (\AA)} = 0.0204 \times [\text{Total Fe (apfu)}] + 19.111 \quad (R^2 = 0.77), \quad (11)$$

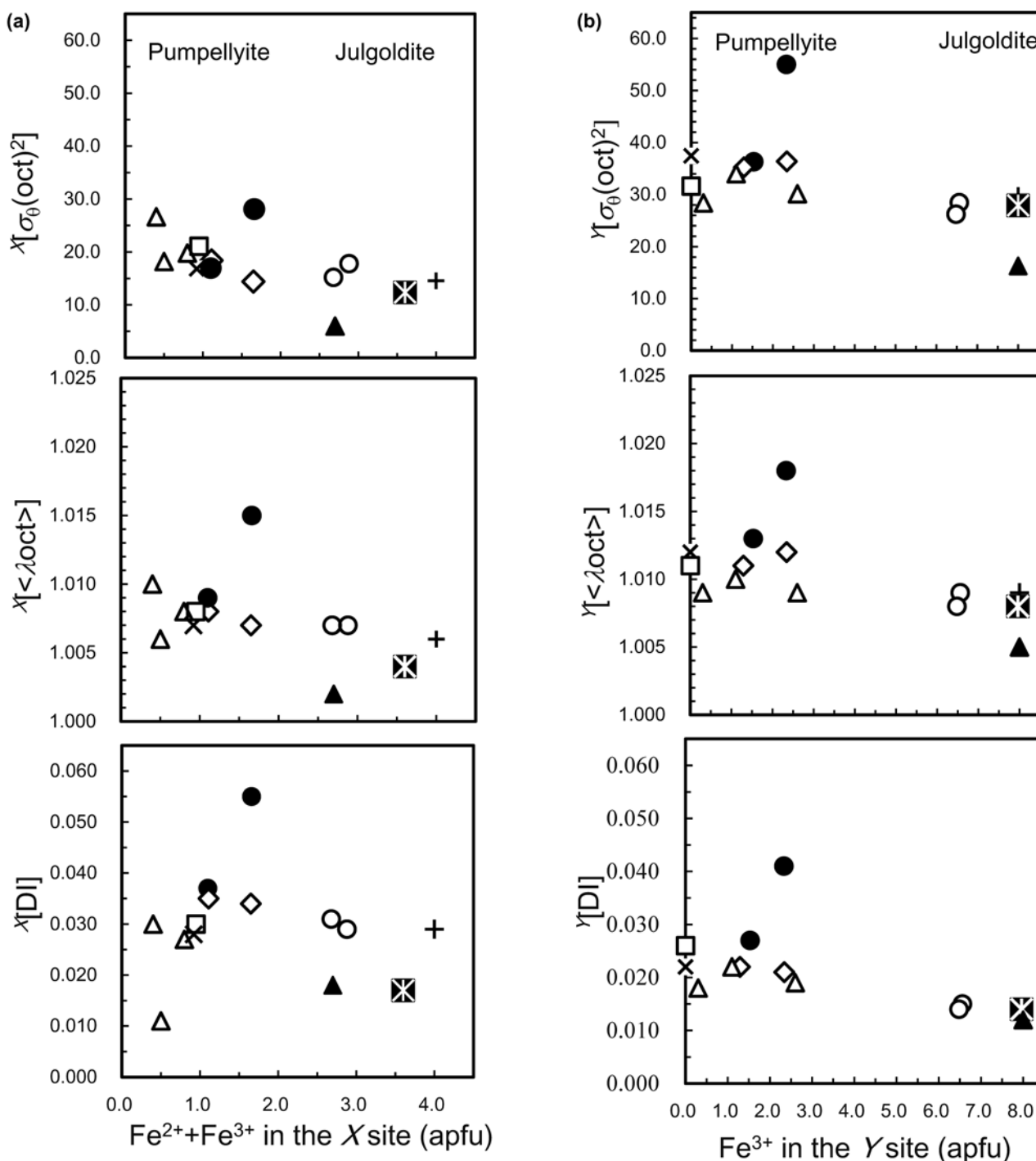


Figure 8. Changes in quadratic elongation $\langle \lambda_{\text{oct}} \rangle$, bond angle variance $\sigma_{\theta}(\text{oct})^2$, and bond length distortion index DI(oct) at the X site versus $\text{Fe}^{2+} + \text{Fe}^{3+}$ (apfu) in the X site (a) and at the Y site (b) versus Fe^{3+} (apfu) in the Y site of pumpellyites and julgoldites listed in Table 9. Closed circle: CLW and CGH pumpellyites in this study with $\chi\text{Fe} = 1.10$ and 1.66 apfu, respectively; open diamond: Nagashima *et al.* (2006); multiplication sign: Yoshiasa and Matsumoto (1985); open square: Galli and Alberti (1969); open triangle: Artioli and Geiger (1994); plus sign: Allmann and Donnay (1973); closed triangle: Artioli *et al.* (2003); open circle: Nagashima *et al.* (2018); closed star: Kasatkin *et al.* (2021).

$$\beta (^{\circ}) = 0.0132 \times [\text{Total Fe (apfu)}] + 97.417 \quad (R^2 = 0.75), \quad \text{and} \quad (12)$$

$$V (\text{\AA}^3) = 4.5647 \times [\text{Total Fe (apfu)}] + 984.22 \quad (R^2 = 0.88). \quad (13)$$

Therefore, the chemical composition and structure results for the CLW and CHG pumpellyites support the proposed interpretation that the change in the size of the XO_6 and YO_6 octahedra caused by the continuous and simultaneous change of $(\text{Fe}^{2+} + \text{Fe}^{3+})$ content in the X site and of Fe^{3+} in the Y site result in the systematic change in structure.

Table 10. Unit-cell parameters and cell volumes of pumpellyite and juldolite in this study and published literature.

Specimen	Total Fe (apfu)	<i>a</i> (Å)	<i>b</i> (Å)	<i>c</i> (Å)	β (°)	<i>V</i> (Å ³)	Reference
Pumpellyite CLW from Chichibu	2.60	8.8456(4)	5.9393(2)	19.1613(8)	97.461(3)	998.14(7)	This study
Pumpellyite CHG from Chichibu	4.21	8.8672(3)	5.9562(2)	19.1899(6)	97.473(2)	1004.9(2)	This study
Pumpellyite from Tokoro, Hokkaido	2.98	8.83(1)	5.939(8)	19.16(2)	97.30(1)	997(3)	Akasaka et al. (1997)
Pumpellyite from Mitsu, Shimane	4.72	8.83(1)	5.944(8)	19.21(2)	97.30(4)	1001(2)	Akasaka et al. (1997)
Pumpellyite MTS from Shimane	3.99	8.8461(1)	5.9657(1)	19.2016(4)	97.462(1)	1004.75(4)	Nagashima et al. (2006)
Pumpellyite KGH from Shimane	2.40	8.8335(3)	5.9381(3)	19.1659(6)	97.446(2)	996.85(6)	Nagashima et al. (2006)
Pumpellyite from Sambagawa, Gumma	0.92	8.812(4)	5.895(2)	19.116(11)	97.41(7)	984.75	Yoshiasa and Matsumoto (1985)
Pumpellyite HR from Hicks Ranch	0.95	8.83(1)	5.90(1)	19.17(2)	97.12(8)	991.00	Galli and Alberti (1969)
Pumpellyite HR from Hicks Ranch	0.77	8.8193(2)	5.9042(2)	19.1138(5)	97.433(2)	986.91(3)	Artioli and Geiger (1994)
Pumpellyite K1 from Keweenawan	1.44	8.8192(2)	5.9192(3)	19.1274(5)	97.446(2)	990.06(49)	Artioli and Geiger (1994)
Pumpellyite BU from Torrente Bulla	3.35	8.8375(2)	5.9520(2)	19.1812(5)	97.461(2)	1000.42(3)	Artioli and Geiger (1994)
Juldolite from Långban	11.1	8.92(1)	6.09(1)	19.37(2)	97.50(8)	1043	Moore (1971)
Juldolite from Långban	11.50	8.922(4)	6.081(3)	19.432(9)	97.60(6)	1044	Allmann and Donnay (1973)
Juldolite from Kilsyth	11.56	8.9360(2)	6.0831(2)	19.4523(5)	97.57(2)	1048.15(4)	Livingstone (1976)
Juldolite from Tafford	9.37	8.949*	6.047*	19.426*	97.63*	1041.92*	Brastad (1984)
Juldolite-(Fe ³⁺) from Bombay	10.69	8.8879(4)	6.0580(2)	19.3321(7)	97.498(2)	1032.01(7)	Artioli et al. (2003)
Juldolite-(Fe ²⁺) from Bombay	9.76	8.9034(4)	6.0568(3)	19.3580(9)	97.584(3)	1034.77(8)	Nagashima et al. (2018)
Juldolite from Kreimbach/Kaulbach	9.16	8.9454(3)	6.0519(2)	19.4008(5)	97.589(2)	1041.10(3)	Nagashima et al. (2018)
Juldolite-(Fe ³⁺) from Crimea	11.56	8.8885(7)	6.0791(4)	19.3679(14)	97.499(4)	1037.58(13)	Kasatkin et al. (2021)

* Errors are not shown in Brastad (1984).

Implication

Empirical estimation of Fe²⁺ and Fe³⁺ contents and cation distributions in the octahedral sites from total Fe contents

Additional precise and accurate data on the intracrystalline distribution of cations and the structural properties of pumpellyite are required for understanding the crystallochemical rule on the distribution of trivalent cations in the octahedral sites of pumpellyite. However, equations 1 and 2, representing the regression lines for the Fe contents at the X and Y sites versus the total Fe content in pumpellyite, and equations 3–6 for the number of cations at the X site versus the total Fe content at the X site, can be used to give an empirical estimation of a structural formula from only EMPA data. Firstly, the Fe contents at the X and Y sites (^XFe and ^YFe, respectively) are estimated using equations 1 and 2; secondly, the Mg, Al³⁺, Fe³⁺, and Fe²⁺ contents in the X site are estimated by applying ^XFe to equations 3–6. For example, by applying total Fe content, 2.49 apfu, in the CLW pumpellyite to equations 1 and 2, ^XFe = 1.05 and ^YFe = 1.43 apfu are calculated; then from ^XFe = 1.05 apfu and equations 3–6, ^XMg = 1.18, ^XAl³⁺ = 1.77, ^XFe³⁺ = 0.42, ^XFe²⁺ = 0.67 apfu are calculated. Finally, the estimated site population at the X and Y sites is written as ^X[Mg_{1.18}Fe_{0.67}Fe_{0.42}Al_{1.77}]_{Σ4.04}^Y[Fe_{1.43}Al_{6.57}]_{Σ8.00} (apfu). Similarly, the site population at the X and Y sites of the CHG pumpellyite with 4.15 apfu total Fe content (EMPA data in Table 1) is estimated as ^X[Mg_{0.92}Fe_{0.76}Fe_{0.83}Al_{1.52}]_{Σ4.03}^Y[Fe_{2.67}Al_{5.33}]_{Σ8.00}.

Alternatively, the Fe³⁺ and Al³⁺ distribution in the X and Y sites can be also estimated by applying *K_D*, defined as (Fe³⁺/Al³⁺)^X/(Fe³⁺/Al³⁺)^Y. Although the *K_D* values in the present study and published ones are somewhat variable, 1.12–1.90, by using the average *K_D* value, *K_D* = 1.52, the Fe³⁺ and Al³⁺ populations in the X and Y sites are calculated to be ^X[Fe_{0.63}Al_{1.70}]^Y[Fe_{1.58}Al_{6.42}] and ^X[Fe_{1.00}Al_{1.39}]^Y[Fe_{2.58}Al_{5.42}] (apfu) for the CLW and CHG pumpellyites, respectively.

The experimentally determined site populations of the CLW and CHG pumpellyites are ^X[Mg_{1.19}Mn_{0.09}Fe_{0.39}Fe_{0.71}Al_{1.62}]^Y[Fe_{1.50}Al_{6.50}] and ^X[Mg_{0.97}Mn_{0.02}Fe_{0.63}Fe_{1.03}Al_{1.36}]^Y[Fe_{2.55}Al_{5.45}] in apfu, respectively (Table 8), which is close to the estimated Fe³⁺ and Al³⁺ contents at the X and Y sites, from applying equations 1–6 and *K_D* values, above. Therefore, if determination

of the intracrystalline distribution of Fe in Fe-rich pumpellyite is not possible because of analytical difficulties, the Fe²⁺ and Fe³⁺ contents and a structural formula, can be derived using the above methods, and help to contribute to understanding its crystallochemical feature.

Empirical estimation of mean <X–O> and <Y–O> distances and unit-cell parameters from Fe contents

Even when X-ray diffraction data of Fe-rich pumpellyite are not available, the site populations at the X and Y sites estimated from total Fe content enable us to predict the mean <X–O> and <Y–O> distances using equations 7 and 8. In the case of CLW pumpellyite with a total Fe content of 2.49 apfu, the mean <X–O> and <Y–O> distances are calculated to be mean <X–O> = 2.023 Å and mean <Y–O> = 1.944 Å, which are very consistent with those determined: 2.040 Å and 1.944 Å, respectively. Furthermore, the estimated mean <X–O> and <Y–O> distances of the CGH pumpellyite with total Fe of 4.15 apfu, mean <X–O> = 2.052 Å and mean <Y–O> = 1.961 Å, are similar to the determined values, <X–O> = 2.060 Å and mean <Y–O> = 1.980 Å (Table 4).

Equations 9–13 enable the estimation of unit-cell parameters from total Fe contents in pumpellyite. Calculated unit-cell parameters of the CLW and CHG pumpellyites are *a* = 8.837, *b* = 5.931, *c* = 19.162 Å and β = 97.45°, resulting in cell volume *V* = 995.6 Å³, and *a* = 8.855, *b* = 5.956, *c* = 19.196 Å and β = 97.47°, with *V* = 1003.2 Å³, respectively, and close to those determined, listed in Table 2.

The unit-cell parameters and mean bond lengths estimated for a pumpellyite for which no structural data are available provide clues about the structural features of the pumpellyite and provide motivation for a future complete analysis of the crystal structure.

Common and unique features of cation distribution in Fe-rich pumpellyite and juldolite

As shown in Fig. 9, the change in unit-cell parameters and lattice volume with Fe content in pumpellyite is linearly related to that in juldolite, which illustrates the commonality of structural changes

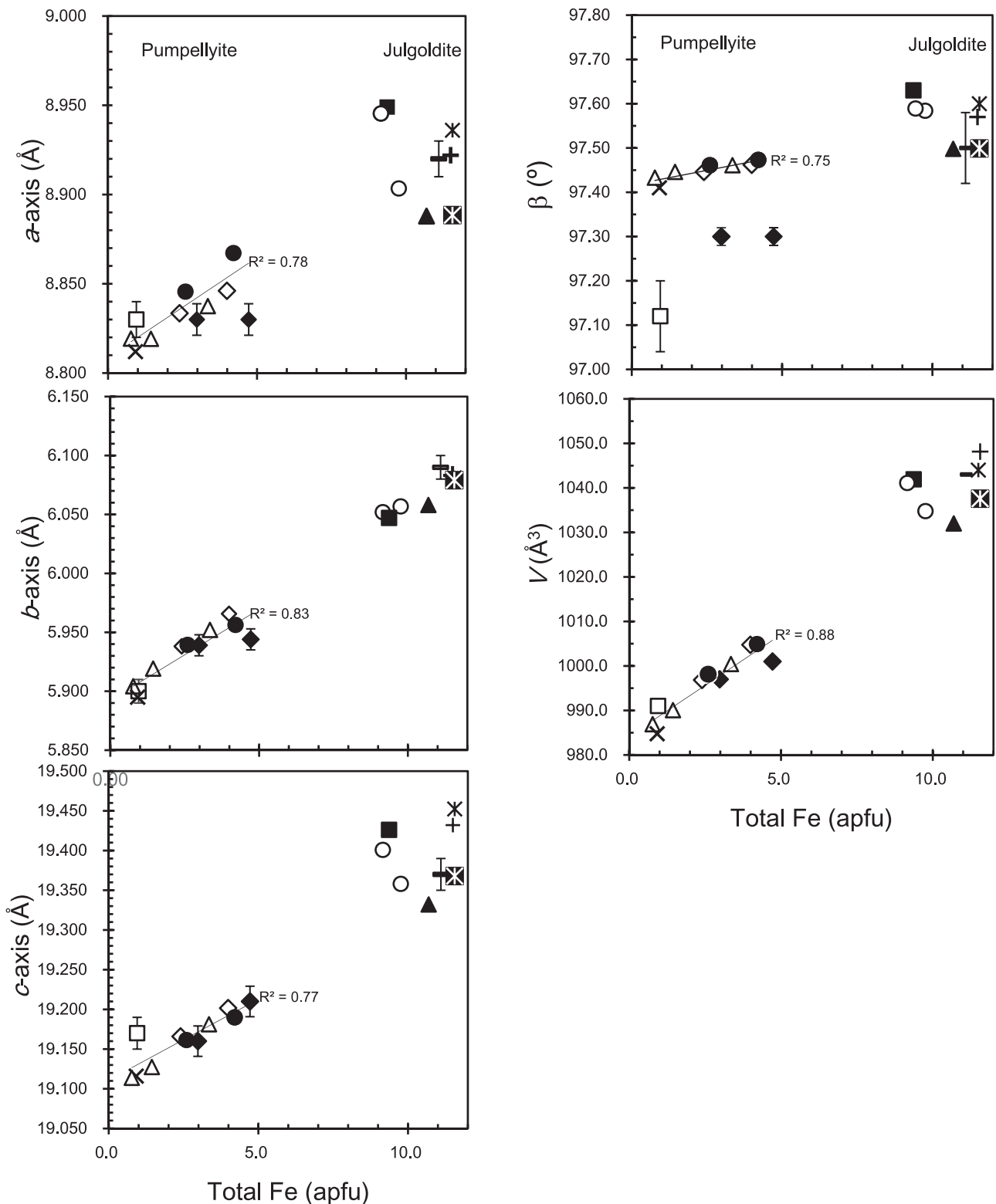


Figure 9. Variation of unit-cell parameters and cell volume versus total Fe (apfu) in pumpellyite and julgoldite listed in Table 10. Closed circle: CLW and CGH pumpellyites in this study with total Fe of 2.60 and 4.21 apfu, respectively; closed diamond: Akasaka *et al.* (1997); open diamond: Nagashima *et al.* (2006); multiplication sign: Yoshiasa and Matsumoto (1985); open square: Galli and Alberti (1969); open triangle: Artioli and Geiger (1994); horizontal bar with error bar: Moore (1971); plus sign: Allmann and Donnay (1973); star: Livingstone (1976); closed square: Brastad (1984); closed triangle: Artioli *et al.* (2003); open circle: Nagashima *et al.* (2018); closed star: Kasatkin *et al.* (2021). Regression lines of unit-cell parameters and cell volume for pumpellyite are represented by equations 9–13 in the document.

with Fe content in pumpellyite and juldite. The change of the mean $\langle Y-O \rangle$ distance versus Fe^{3+} content in the Y site also shows a common structural feature in pumpellyite and juldite: the mean $\langle Y-O \rangle$ distances of juldites are on the extension of the regression line of the mean $\langle Y-O \rangle$ distance versus Fe^{3+} in the Y site of pumpellyite (Fig. 7b). However, as shown in Fig. 7a, the variation trend of the mean $\langle X-O \rangle$ distance versus $(Fe^{2+}+Fe^{3+})$ of the X site in pumpellyite does not lead linearly to that of juldite, because the increasing rate of the mean $\langle X-O \rangle$ distance in juldite, $0.0126 \text{ \AA} / X[Fe^{2+}+Fe^{3+}] \text{ apfu}$, is significantly smaller than $0.056 \text{ \AA} / X[Fe^{2+}+Fe^{3+}] \text{ apfu}$ of pumpellyite (equation 8), and rather close to the gradient of the mean $\langle Y-O \rangle$ distance of pumpellyite and juldite, $0.014 \text{ \AA} / Y[Fe^{3+}]$ (equation 7). As the increase of the mean $\langle X-O \rangle$ distance in pumpellyite is due to the increase of both Fe^{2+} and Fe^{3+} in the X site, and the mean $\langle Y-O \rangle$ distance increases with the substitution of Fe^{3+} for Al^{3+} , the increasing rate of the mean $\langle X-O \rangle$ distance versus $X[Fe^{2+}+Fe^{3+}]$ of juldite suggests an increase of Fe^{3+} in the X site. On this basis, almost half of the X sites in juldite are filled initially with Fe^{2+} , and the subsequent increase in Fe^{3+} in juldite leads to an increase in Fe^{3+} at the X sites. As shown in Table 8 and Fig. 6, Mg and Al in juldite decrease along the $X[Mg - X[Fe^{2+}+Fe^{3+}]]$ and $X[Al - X[Fe^{2+}+Fe^{3+}]]$ trends of pumpellyite, respectively, and become almost nil in juldites with $X[Fe^{2+}+Fe^{3+}] > 3$. However, in contrast to the systematic variation of Fe^{2+} and Fe^{3+} in the X site of pumpellyites, the reported Fe^{2+} and Fe^{3+} contents in the X site of juldites are significantly variable (Table 8; Fig. 6). Thus, the above interpretation on the different variation trend of the mean $\langle X-O \rangle$ distance versus $X[Fe^{2+}+Fe^{3+}]$ between pumpellyite and juldite is not certain at present, and further data on Fe^{2+} and Fe^{3+} contents and their site populations are required.

Conclusions

Intracrystalline distribution of cations and structural properties of two Fe-rich pumpellyites with average total Fe_2O_3 contents of 10.01(169) and 16.07(108) wt.%, separated from green rocks, subjected to prehnite–pumpellyite-facies metamorphism, of the Kanogawa unit, the northern Chichibu belt, western Shikoku, have been clarified. The determined structural formula of the former is $W(Ca_{7.96}Na_{0.01}K_{0.02})_{\Sigma 7.99}X(Mg_{1.19}Mn_{0.2}^{2+}Fe_{0.39}^{2+}Fe_{0.71}^{3+}Al_{1.62})_{\Sigma 4.00}Y(Al_{6.47}Fe_{1.50}^{3+}V_{0.02}Ti_{0.01})_{\Sigma 8.00}Si_{12.26}O_{43.33}(OH)_{12.67}$, and that of the latter is $W(Ca_{8.01}K_{0.01})_{\Sigma 8.02}X(Mg_{0.97}Mn_{0.2}^{2+}Fe_{0.63}^{2+}Fe_{1.03}^{3+}Al_{1.36})_{\Sigma 4.01}Y(Al_{5.44}Fe_{2.55}^{3+}V_{0.01})_{\Sigma 8.00}Si_{12.02}O_{42.69}(OH)_{13.31}$, and, thus, the former and the latter are identified as pumpellyite-(Al). The distribution coefficients of Fe^{3+} versus Al^{3+} between the X and Y sites are $K_D = 1.62$ and 1.90 for the former and latter, respectively, implying a stronger preference for Fe^{3+} in the X site than Al^{3+} . The results of the present study and published studies for Fe-rich pumpellyites indicate that Mg^{2+} and Al^{3+} in the X site decrease linearly (equations 3 and 4) and $[Fe^{2+} + Fe^{3+}]$ increase instead (equation 1), but the increase of Fe^{3+} is more significant than Fe^{2+} (equations 5 and 6), whereas, in the Y site, Fe^{3+} increases linearly versus total Fe in pumpellyite (equation 2). The average interatomic distances at the X and Y sites correlate well with the $[Fe^{2+} + Fe^{3+}]$ in the X site (equation 8) and Fe^{3+} in the Y site (equation 7), respectively, and the unit-cell parameters and cell volume change linearly versus total Fe in pumpellyite (equations 9–13). Those relationships are applicable for the estimation of cation contents, including Fe^{2+} and Fe^{3+} , in the X and Y sites and of the structural features, such as mean bond lengths at the

octahedral sites and the unit-cell parameters, from total Fe content in pumpellyite. In addition, the systematic variation of cation population and structural features for Fe content in pumpellyite helps to evaluate the relationship between Fe content and cation distribution and structural properties in juldite.

Acknowledgements. This paper is based on a master thesis study by Y. Goishi (Imaizumi) when she was a student at the Department of Geoscience, Graduate School of Science and Engineering, Shimane University. Y. Goishi (Imaizumi) and M. Akasaka thank Drs. Maki Hamada (present affiliation: Kanazawa University) and Terumi Ejima (present affiliation: Shinshu University) for their help with field investigation and collecting samples, and Dr. Mariko Nagashima of Yamaguchi University for her helpful discussion and advice for the investigation of Fe-rich pumpellyite and X-ray Rietveld refinement. Thanks to the late Dr. Fujio Izumi of the National Institute for Materials Science and Dr. Koichi Momma of the National Museum of Nature and Science for their permission to use the RIETAN-FP and VESTA programs. This paper is dedicated to the late Dr. Kenji Togari (Professor of Hokkaido University), the late Dr. Teruo Watanabe (Professor of Hokkaido University), the late Dr. Kenzo Yagi (Professor emeritus of Hokkaido University and Tohoku University), the late Dr. Kosuke Onuma (Professor emeritus of Tohoku University), and the late Dr. Jiro Ishii (Professor of Tokai University), who had guided and supported M.A. for many years.

Supplementary material. The supplementary material for this article can be found at <https://doi.org/10.1180/mgm.2023.80>.

Competing interests. The authors declare none.

References

- Akasaka M. and Shinno I. (1992) Mössbauer spectroscopy and its recent application to silicate mineralogy. *Journal of Mineral Society of Japan*, **21**, 3–20. [in Japanese]
- Akasaka M., Sakakibara M. and Togari K. (1988) Piemontite from the manganese hematite ore deposits in the Tokoro Belt, Hokkaido, Japan. *Mineralogy and Petrology*, **38**, 105–116.
- Akasaka M., Kimura Y., Omori Y., Sakakibara M., Shinno I. and Togari K. (1997) ^{57}Fe Mossbauer study of pumpellyite-okhotskite-juldite series minerals. *Mineralogy and Petrology*, **61**, 181–198.
- Akasaka M., Takasu Y., Handa M., Nagashima M., Hamada M. and Ejima T. (2019) Distribution of Cr^{3+} between octahedral and tetrahedral sites in synthetic blue and green $(CaMgSi_2O_6)_{95}(CaCrAlSiO_6)_5$ diopside. *Mineralogical Magazine*, **83**, 497–505.
- Allmann R. and Donnay G. (1971) Structural relations between pumpellyite and ardenite. *Acta Crystallographica*, **B27**, 1871–1875.
- Allmann R. and Donnay G. (1973) The crystal structure of juldite. *Mineralogical Magazine*, **39**, 271–281.
- Artoli G. and Geiger CA. (1994) The crystal chemistry of pumpellyite: An X-ray Rietveld Refinement and ^{57}Fe Mossbauer Study. *Physics and Chemistry of Minerals*, **20**, 443–453.
- Artoli G., Geiger CA. and Dapiaggi M. (2003) The crystal chemistry of juldite- Fe^{3+} from Bombay, India, studied using synchrotron X-ray powder diffraction and ^{57}Fe Mössbauer spectroscopy. *American Mineralogist*, **88**, 1084–1090.
- Bancroft G.M. (1973) *Mössbauer Spectroscopy. An Introduction for Inorganic Chemists and Geochemists*. McGraw-Hill, London.
- Baur W.H. (1974) The geometry of polyhedral distortions. Predictive relationships for the phosphate group. *Acta Crystallographica*, **B30**, 1195–1215.
- Brastad K. (1984) Juldite from Tafjord Sunnmøre. Contribution to the Mineralogy of Norway, No. 67. *Norsk Geologisk Tidsskrift*, **64**, 251–255.
- Brese N.E. and O’Keeffe M. (1991) Bond-valence parameters for solids. *Acta Crystallographica*, **B47**, 192–197.
- Brigatti M.F., Caprill E., and Marchesini M. (2006) Poppiite, the V^{3+} end-member of the pumpellyite group: Description and crystal structure. *American Mineralogist*, **91**, 584–588.

- Brown I.D. and Altermatt D. (1985) Bond-valence parameters obtained from a systematic analysis of the Inorganic Crystal Structure Database. *Acta Crystallographica*, **A29**, 266–282.
- Brown I.D. and Shannon R.D. (1973) Empirical bond-strength–bond-length curves for oxides. *Acta Crystallographica*, **A29**, 266–282.
- Coombs D.S. (1953) The pumpellyite mineral series. *Mineralogical Magazine*, **30**, 113–135.
- Coombs D.S., Nakamura Y. and Vuagnat M. (1976) Pumpellyite-actinolite facies schists of the Taveyenne Formation near Loeche, Valais, Switzerland. *Journal of Petrology*, **17**, 440–471.
- Deer W.A., Howie R.A. and Zussman J. (1986) *Rock-forming minerals. 1B (Second edition), Disilicates and ring silicates*. Geological Society Publishing House, UK, pp. 629.
- De Grave E., Vandenbruwaene I. and Van Bockstael M. (1987) ^{57}Fe Mössbauer spectroscopic analysis of chlorite. *Physics and Chemistry of Minerals*, **15**, 173–180.
- Dollase W.A. (1986) Correction of intensities for preferred orientation in powder diffractometry: application of the March model. *Journal of Applied Crystallography*, **19**, 267–272.
- Evarts R.C. and Schiffman P. (1983) Submarine hydrothermal metamorphism of the Del Puerto ophiolite, California. *American Journal of Science*, **283**, 289–340.
- Galli E. and Alberti A. (1969) On the crystal structure of pumpellyite. *Acta Crystallographica*, **B25**, 2276–2281.
- Gandolfi G. (1967) Discussion upon methods to obtain X-ray «powder patterns» from a single crystal. *Mineralogica et Petrographica Acta*, **13**, 67–74.
- Gottardi G. (1965) Die kristallstruktur von pumpellyit. *Tschermaks Mineralogische und Petrographische Mitteilungen, series 3*, **10**, 115–119.
- Hamada M., Seto (Sakamoto) S., Akasaka M. and Takasu A. (2008) Chromian pumpellyite and associated chromian minerals from Sangun metamorphic rocks, Osayama, southwest Japan. *Journal of Mineralogical and Petrological Sciences*, **103**, 390–399.
- Hamada M., Akasaka M., Seto S. and Makino K. (2010) Crystal chemistry of chromian pumpellyite from Osayama, Okayama Prefecture, Japan. *American Mineralogist*, **95**, 1294–1304.
- Hashimoto, M. and Kashima, N. (1970) Metamorphism of Paleozoic greenstones in the Chichibu Belt of western Shikoku. *The Journal of Geological Society of Japan*, **76**, 199–204.
- Hill R.J. and Flack H.D. (1987) The use of the Durbin–Watson d statistic in Rietveld analysis. *Journal of Applied Crystallography*, **20**, 356–361.
- Ivanov O.K., Arkhangel'skaya V.A., Miroshnikova L.O. and Shilova T.A. (1981) Shuiskite, the chromium analogue of pumpellyite from the Bisersk deposit, Urals. *Zapiski Vserossiyskogo Mineralogicheskogo Obshchestva*, **110**, 508–512 [in Russian].
- Izumi F. (1993) Rietveld analysis program RIETAN and PREMOS and special applications. Pp. 236–253 in: *The Rietveld Method* (R.A. Young, editor). Oxford Science Publications, UK.
- Izumi F. and Momma K. (2007) Three-dimensional visualization in powder diffraction. *Solid State Phenomena*, **130**, 15–20.
- Kano K., Satoh H. and Bunno M. (1986) Iron-rich pumpellyite and prehnite from the Miocene gabbroic sills of the Shimane Peninsula, southwest Japan. *Journal of Japanese Association of Mineralogy, Petrology, and Economic Geology*, **81**, 51–58.
- Kasatkin A.V., Zubkova N. V., Chukanov N. V., Ksenofontov D. A., Shkoda R., Tishchenko A.I., Voronin M.V., Britvin S.N. and Pekov, I. V. (2021) Unusually rich in iron julgoldite-(Fe^{3+}) from the Karadag volcanic massifs (Crimean Peninsula). *Zapiski RMO*, **150**, 96–112.
- Kashima N. (1969) Stratigraphical studies of the Chichibu belt in Western Shikoku. *Memoirs of the Faculty of Science, Kyushu University, Ser. D, Geology*, **Vol. XIX**, **3**, 387–436.
- Kihara K. (1990) An X-ray study of the temperature dependence of the quartz structure. *European Journal of Mineralogy*, **2**, 63–77.
- Liou J.G. (1979) Zeolite facies metamorphism of basaltic rocks from the east Taiwan ophiolite. *American Mineralogist*, **64**, 1–14.
- Livingstone A. (1976) Julgoldite, new data and occurrences; a second recording. *Mineralogical Magazine*, **40**, 761–763.
- Matsuoka A., Yamakita S., Sakakibara M. and Hisada K. (1998) Unit division for the Chichibu Composite Belt from a viewpoint of accretionary tectonics and geology of western Shikoku, Japan. *Journal of Geological Society of Japan*, **104**, 634–653 [in Japanese].
- Mevel C. (1981) Occurrence of pumpellyite in hydrothermally altered basalts from the Vema Fracture Zone (Mid-Atlantic Ridge). *Contributions to Mineralogy and Petrology*, **76**, 386–393.
- Minakawa T. (1992) Study on characteristic mineral assemblages and formation process of metamorphosed manganese ore deposits in the Sanbagawa belt. *Memoirs of the Faculty of Science of Ehime University*, **1**, 1–74 [in Japanese with English abstract].
- Momma K. and Izumi F. (2011) VESTA 3 for three-dimensional visualization of crystal, volumetric and morphology data. *Journal of Applied Crystallography*, **44**, 1272–1276.
- Moore PB (1971) Julgoldite, the Fe^{2+} – Fe^{3+} dominant pumpellyite. A new mineral from Långban, Sweden. *Lithos*, **4**, 93–99.
- Nagashima M. and Akasaka M. (2007) The distribution of chromium in chromian pumpellyite from Sarani, Urals, Russia: A TOF neutron and X-ray Rietveld study. *The Canadian Mineralogist*, **45**, 837–846.
- Nagashima M., Ishida T. and Akasaka M. (2006) Distribution of Fe among octahedral sites and its effect on the crystal structure of pumpellyite. *Physics and Chemistry of Minerals*, **33**, 178–191.
- Nagashima M., Akasaka M., Ikeda K., Kyono A. and Makino K. (2010) X-ray single-crystal and optical spectroscopic study of chromian pumpellyite from Sarany, Urals, Russia. *Journal of Mineralogical and Petrological Sciences*, **105**, 187–193.
- Nagashima M., Cametti G. and Armbruster, T. (2018) Crystal chemistry of julgoldite, a mineral series of the pumpellyite group: re-investigation of Fe distribution and hydrogen-bonding. *European Journal of Mineralogy*, **30**, 721–731.
- Nakamura Y. (1993) The determination of lattice parameters of a small crystal with a Gandolfi camera. *Journal of Mineralogical Society of Japan*, **22**, 113–122 [Japanese with English abstract].
- Nakamura Y. (1999) Precise analysis of a very small mineral by an X-ray diffraction method. *Journal of Mineralogical Society of Japan*, **28**, 117–121 [Japanese with English abstract].
- Palache C. and Vassar H.E. (1925) Some minerals of the Keweenaw copper deposits: pumpellyite, a new mineral; sericite; saponite. *American Mineralogist*, **10**, 412–418.
- Passaglia E. and Gottardi G. (1973) Crystal chemistry and nomenclature of pumpellyites and julgoldites. *The Canadian Mineralogist*, **12**, 219–223.
- Phillips M.W., Draheim J.E., Popp R.K., Clowe C.A. and Pinkerton A.A. (1989) Effects of oxidation-dehydrogenation in tschermakitic hornblende. *American Mineralogist*, **74**, 764–773.
- Post, J.E. and Bish, D.L. (1989) Rietveld refinement of crystal structures using powder X-ray diffraction data. Pp. 277–308 in: *Modern Powder Diffraction* (Bish, D.L. and Post, J.E., editors). Reviews in Mineralogy, 20. Mineralogical Society of America, Washington, DC, USA.
- Robinson K., Gibbs G.V. and Ribbe P.H. (1971) Quadratic elongation: a quantitative measure of distortion in coordination polyhedra. *Science*, **172**, 567–570.
- Sakakibara M. (1986) A newly discovered high-pressure terrane in eastern Hokkaido, Japan. *Journal of Metamorphic Geology*, **4**, 401–408.
- Sakakibara M. (1991) Metamorphic petrology of the Northern Tokoro metabasites, eastern Hokkaido, Japan. *Journal of Petrology*, **32**, 333–364.
- Sakakibara M., Oyama Y., Umeki M., Sakakibara H., Shono H. and Goto S. (1998) Geotectonic division and regional metamorphism of Northern Chichibu Belt in western Shikoku, Japan. *Journal of Geological Society of Japan*, **104**, 604–622 [in Japanese].
- Sakakibara M., Umeki M. and Cartwright I. (2007) Isotopic evidence for channelled fluid flow in low-grade metamorphosed Jurassic accretionary complex in the Northern Chichibu belt, western Shikoku, Japan. *Journal of Metamorphic Geology*, **25**, 383–400.
- Schiffman P. and Liou J.G. (1980) Synthesis and stability relations of Mg-Al pumpellyite, $\text{Ca}_4\text{Al}_5\text{MgSi}_6\text{O}_{21}(\text{OH})_7$. *Journal of Petrology*, **21**, 441–474.
- Schiffman P. and Liou J.G. (1983) Synthesis of Fe-pumpellyite and its stability relations with epidote. *Journal of Metamorphic Geology*, **1**, 91–101.
- Shannon R.D. (1976) Revised effective ionic radii and systematic studies of interatomic distances in halides and chalcogenides. *Acta Crystallographica*, **A32**, 751–767.

- Togari K. and Akasaka M. (1987) Okhotskite, a new mineral, an Mn³⁺-dominant member of the pumpellyite group, from the Kokuriki mine, Hokkaido, Japan. *Mineralogical Magazine*, **51**, 611–614.
- Togari K., Akasaka M., Sakakibara M. and Watanabe T. (1988) Mineralogy of manganiferous iron ore deposits and chert from the Tokoro Belt, Hokkaido. *Mining Geology Special Issue*, **No. 12**, 115–126.
- Umeki M. and Sakakibara M. (1998a) Geology and petrologic study of basic rocks of Northern Chichibu Belt in the Hijikawa district, western Shikoku, Japan. *Journal of Geological Society of Japan*, **104**, 590–603 [in Japanese].
- Umeki M. and Sakakibara M. (1998b) Biotite-bearing basic semischists from the northern Chichibu belt in the Hijikawa district *Journal of Japanese Association of Mineralogy, Petrology and Economic Geology*, **93**, 291–306 [in Japanese].
- Yabuta W. and Hirajima T. (2020) A new occurrence of okhotskite in the Kurosegawa belt, Kyushu, Japan: the okhotskite + Mn-lawsonite assemblage as a potential high-pressure indicator. *Journal of Mineralogical and Petrological Sciences*, **115**, 431–439.
- Yoshiasa A. and Matsumoto T. (1985) Crystal structure refinement and crystal chemistry of pumpellyite. *American Mineralogist*, **70**, 1011–1019.
- Young R.A. (1993) Introduction to the Rietveld method. Pp. 1–38 in: *The Rietveld Method* (Young R.A., editor). Oxford Science Publications, UK.